Egypt. J. Geo. **Vol. 67,** pp: 299-319 (2023)

Egyptian Journal of Geology

https://egjg.journals.ekb.eg

Depositional environment and paleoclimate of the Middle Jurassic sedimentary rocks in Matruh Basin, Northwestern Desert, Egypt

Walaa A. Ali [1*]

[*1] *Petroleum Geology Department, Faculty of Petroleum and Mining Sciences, Matrouh University, 51511, Matrouh, Egypt*

THIS study investigates the depositional environment and paleoclimate conditions of the Middle Jurassic Khatatba Formation in Matruh Basin, northwestern Egypt, which represents an important regional gas producer in the East Mediterranean province. Khatatba Fm is marked by in situ dual source and reservoir characteristics, where fluctuations of fine and coarse clastics form intra-formational sources (lithology: shale and argillaceous siltstones), where TOC wt%: 0.88–12.98, avg. 2.95, in Matruh-5 and TOC wt%: 0.80–6.99, avg. 2.26, in Matruh-6 wells, respectively. Yet, reservoir rocks (Lithology: sandstone) were deposited during semi-arid and semi-humid conditions. This in situ dual performance is related to Tethyan sea level oscillations and climate changes during the Middle Jurassic. The Tethyan rifting that occurred during the Late Jurassic and Early Cretaceous caused subsidence events, which were accordingly associated with source rock maturation. Studying the provenance and sedimentation conditions responsible for the accumulation of organic-rich and organic-poor deposits in the Khatatba Formation in the Matruh Basin. Therefore, inorganic geochemical and geophysical data were used to interpret the depositional environment. Clastics of the Khatatba Formation were sourced by moderate weathering in the target wells of the current study (chemical index of alteration = CIA: avg. 70 and avg. 59, index of chemical variability = ICV: avg. 1.1 and avg. 1.8, chemical index of weathering = CIW: avg. 77.8 and avg. 64.7) for Matruh-5 and Matruh-6 wells, respectively. Moreover, the Rb/Sr ratios (avg. 0.36, 0.29 in Matruh-5 and Matruh-6 wells, respectively) have been used to figure out how much chemical weathering happened in the sediments' source area, which is classified as moderate weathering. The K_2O/Al_2O_3 elemental ratios (avg. 0.14 in both wells) are below 0.4, which suggests sediment maturation. Besides, the K_2O/Al_2O_3 ratios were also utilized to infer chemical weathering in the target wells, where values suggest a moderate level of weathering in the area where the parent rocks were situated as well. Within the Matruh-5 and Matruh-6 wells, there is a strong correlation between high levels of strontium (Sr) and low levels of calcium (Ca) in this particular sediment type of Khatatba Fm. This explains why these deposits were accumulated in tide-dominated deltaic environments based on salinity, where Sr/Ca ratios have been used as an indicator of salinity. Moreover, the negative correlations of Ti with Al in the Matruh-5 well (R^2= 0.1139 U.Safa; R^2=0.0007 L.Safa) suggest no association with aluminosilicate clay minerals. While the strong positive correlations of Ti with Al in Matruh-6 well (R^2= 0.858 in U.Safa; R^2= 0.946 in L.Safa) indicate the association of the aluminosilicate minerals. Khatatba Fm Deposition occurred during relatively semi-arid conditions (Sr/Cu: avg. 10.03; 11.33; Rb/Sr: avg. 0.36; 0.29), which were characterized by higher terrigenous inputs (sediment influx (Al/Ca): avg. 4.47, Matruh-5 well; 3.87, Matruh-6 well). Normal salinity conditions accumulated under mostly oxic to suboxic-anoxic settings, where ($100*MgO/Al_2O_3$: avg. 8.48, Matruh-5 well; 11.37, Matruh-6 well), (V/(V + Ni): avg. 0.58 in Matruh-5 well; avg. 0.32 in Matruh-6 well), and Cu/Zn: avg. 0.34 Matruh-5 well; avg. 0.27 Matruh-6 well).

Keywords: Depositional Environment, Paleoclimate, XRF elemental Analysis, Source Rocks, Khatatba Fm Matruh Basin.

*Corresponding author e-mail: walaa.ali@mau.edu.eg
Received: 06/12/2023; Accepted: 30/12/2023
DOI: 10.21608/EGJG.2024.256634.1066

1. Introduction

The structural evolution of Egypt was shaped by various tectonic events that reactivated the pre-existing four main structural orientations, specifically north-south, northeast-southwest, east-northeast-west-southwest, and east-west, inside the underlying bedrock, as documented by **Hantar (1990).** The North African/Arabian Plate and the European Plate underwent a separation process in the Jurassic period, leading to the creation of numerous rift basins **(Dolson et al., 2001).** Due to the convergence of the aforementioned plates, Egypt experienced compressional forces in the NW-NNW and SE-SSE directions. These forces have led to the development of the Syrian Arc System during the Late Cretaceous period. During the Eocene epoch, a compressional stresses led to the uplift and folding of large areas of the North Western Desert in NE to ENE-SW to WSW directions **(Hussein and Abd-Allah., 2001).**

During the earliest Jurassic period, the northern region of Egypt experienced arid conditions and underwent erosion. The lowermost strata of the Middle Jurassic in this region consist of both terrestrial and marine sedimentary deposits. The uppermost strata of the Middle Jurassic consist of carbonate sediments that were deposited in shallow marine environments in the northern basinal areas. This deposition marked the peak of the Jurassic transgression over the eastern regions of the northern Western Desert. The deposition of marine carbonates was the dominant process in the extreme northern region (**Dolson et al., 2000**). The Matruh Basin was originated in the Late Jurassic to Early Cretaceous period and it is a component of the Unstable Shelf. Its geologic feature is a graben, which is a type of down-dropped block of the Earth's crust, and it has a NNE–SSW orientation.
The basin is located between longitudes 26° and 27° 30′ E and latitudes 31° and 31° 17’ N **(Fig. 1 A).** The mentioned area is a section of the northeastern African Craton, which experienced significant tectonic activity throughout the Paleozoic and Mesozoic eras (**Guiraud et al., 2001**). **Sestini (1994)** proposed that the Matruh Basin likely originated as a unified rift during the Permo-Triassic period and subsequently evolved into a pull-apart structure. According to **Meshref (1999)**, the Matruh Basin evolved as a rift basin during the late Cimmerian Orogeny due to the separation of the northern African Plate from the European Plate. **Meshref and Hammouda (1990), Abdel Halim and Moussad (1992),** and **Avseth and Bachrac (2005)** categorized the Matruh Basin as a single gigantic continental basin comprising the Matruh–Shushan Basin.

1.1. Location

The studied area deals with the Matruh Basin, which is part of the Khalda concession, in the northern Western Desert of Egypt. The data set used herein is from the Matruh-5 and Matruh-6 wells in the Matruh Field. The Matruh Field research area is approximately 28.47 square kilometres and is situated 45 kilometres southeast of Matruh city in the north-western region of the Western Desert. The Matruh Field was first identified in 1991 during the drilling of the Matruh 1-1X well **(Fig. 1B).** The well logs indicated the presence of hydrocarbon-rich areas in both the Upper and Lower Safa reservoirs, leading to the finding of gas and condensate. Matruh-5 is located around 500 meters NE from the Matruh-1-1 site, with an estimated drainage radius of 640 meters. The estimated reserves of the Matruh-5 well are around 6 billion cubic feet (BCF) of natural gas and 420 thousand stock tank barrels (MSTB) of condensate, with a condensate-to-gas ratio (CGR) of 70 stock tank barrels per million standard cubic feet (STB/MMSCF). The well Matruh-5 was drilled as a gas development well. Its main purpose was to produce from the Upper Safa reservoirs, with the Lower Safa reservoirs being a secondary target. On the other hand, the proposed site for Matruh-6 well is situated around 820 meters NE of the Matruh-5 location and 1290 meters NE Matruh 1-1. To sum up, Matruh Field produces mainly gas and condensate from the Jurassic Upper and Lower Safa reservoirs.

The important of the present study is to know the provenance and sedimentation conditions responsible for accumulation of organic-rich deposits of the Middle Jurassic Khatatba Formation in the Matruh Basin, North Western Desert of Egypt, which considers as the main gas producer in the East Mediterranean region. Inorganic geochemical and geophysical data was used to interpret the paleoclimate, salinity, and depositional environment.

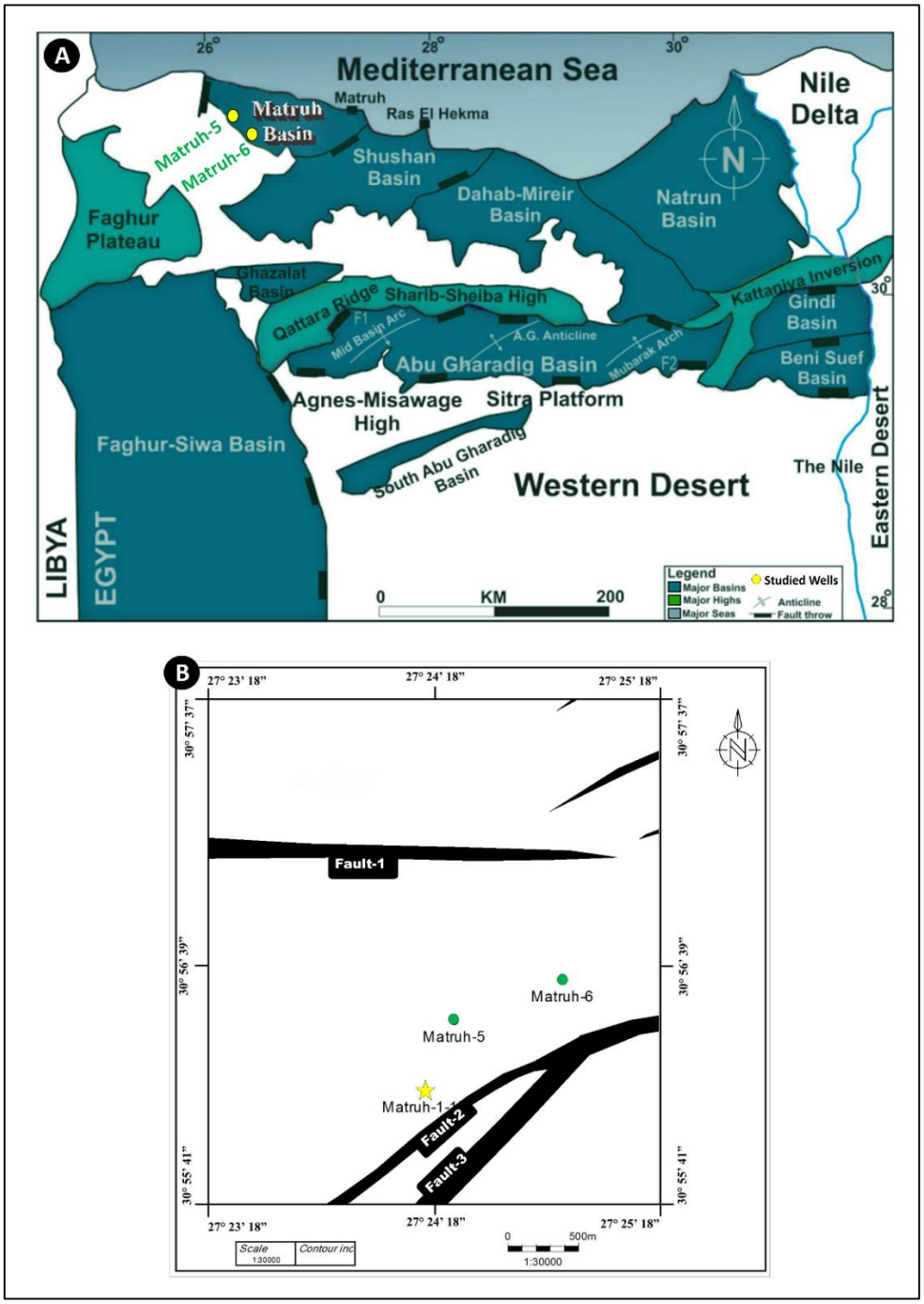

Fig. 1 (A). The map shows the location of the Matruh Basin, as well as other Mesozoic basins in the North Western Desert of Egypt. It also indicates the position of the Matruh-5 and Matruh-6 wells, which are the focus of the current study. The map is based on modified versions of sources from EGPC (1992) and Mansour et al. (2023). (B): Location map of the examined wells and the primary faults in the Matruh Field (After Khalda, 2010).

1.2. Lithostratigraphy

The sedimentary layers in the northern Western Desert including those in the Matruh Basin, are categorized into four main depositional sequences (DSQ) as shown in Figure 2. DSQ1 denotes the main phase of regression during the Early-Middle Jurassic era, distinguished by the presence of sediments originating from fluvio-deltaic and shallow marine environments. DSQ2 represents the main phase of

regression during the Early-middle Cretaceous era, during which sediments from fluvio-deltaic and shallow marine habitats were deposited. DSQ3 denotes a significant period of transgression that took place in the Late Cretaceous. It is distinguished by the accumulation of open marine shale and carbonates. DSQ4 is a notable period of transgression that occurred between the late Paleogene and early Neogene periods. It involved the deposition of open marine shales and carbonates in northern Egypt, which was caused by Miocene regional folding and basin inversion. This information is supported by studies conducted by **Sultan and Halim in 1988**, as well as **Moustafa et al. in 2002**.

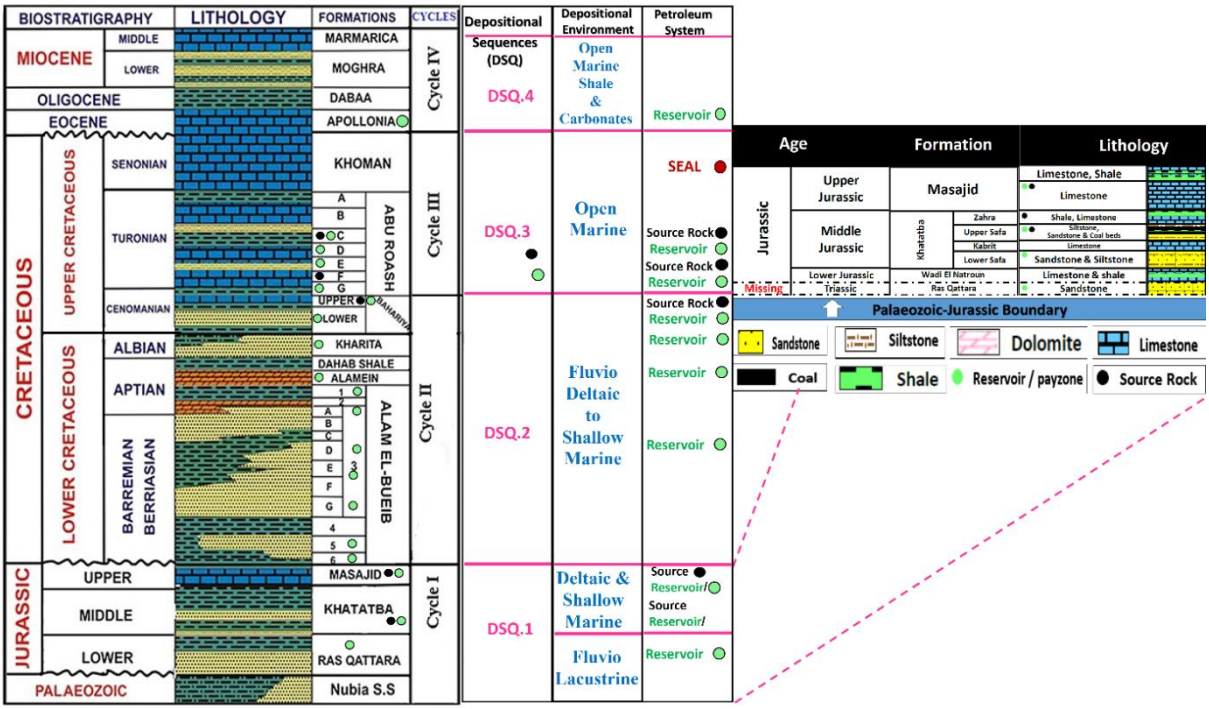

Fig. 2. Stratigraphic column of the Matruh Basin in the North Western Desert of Egypt. It illustrates four primary depositional sequences, providing information on the lithology, age, depositional conditions, and petroleum system features of the formations (modified After EGPC, 1992; Shalaby et al., 2014).

2. Materials and Methods

2.1 Samples

30 drill cuttings samples from the Matruh-5 and Matruh-6 wells were collected from the Khatatba Formation, covering the entire thickness of the Matruh field. These samples from the Middle Jurassic Khatatba Formation were collected from the two wells (Matruh-5, Matruh-6) **(Table 1).** The investigated section ranges in thickness from 1000 ft-1100 ft. The wells are located in the Matruh Field inside the Matruh Basin, namely at coordinates 27° 23’ 18” - 27° 25’ 18” E and 30° 55’ 41” - 30° 57’ 37” N. They have been drilled to a total depth of 15850 ft, 15650, ft in Matruh-5 and Matruh-6 respectively.

2.2. Lithology identification from wireline logs

The analyses of the wireline logs data of the Khatatba Formation in the Matruh-5 and Matruh-6 wells were made to identify the main lithology to help in the interpretations of the paleoenvironments. The lithological composition of the Middle Jurassic Khatatba Formation was determined using wireline and cuttings of mud logs. Density–Neutron crossplots are commonly employed for lithology determination and accurate assessment of matrix porosity in carbonate rocks (**Poupon and Leveaux, 1971**). The “Neutron porosity-Bulk density” cross plot was used and calibrated with Schlumberger cross plot chart to identify the main lithology for the studied formation. Each member was examined separately for better results. The density–neutron cross plots of the Lower and Upper Safa members in both wells show mixed

lithology of sandstones, shale, siltstone, and carbonates.

Before estimating the main lithology of the examined section, correction for shale effect, gas effects have been done. The mud log was used to check the interpretation from the electric log after calculating the depth shift (28 ft / Matruh-5 well; 45 ft/ Matruh-6 well) between the recorded depths of Electric and Mud logs. Because uranium is a radioactive mineral, there is a high gamma-ray (GR) response in front of sandstone or carbonate intervals. When the density-neutron is clean in front of these intervals, it is possible to confirm that the increase in GR observed in front of sandstone and carbonate was caused by uranium rather than the shale effect. Shale, on the other hand, has high GR values in source rock intervals due to its high uranium percentage.

2. 3. XRF Elemental Analysis

The selected samples were finely ground and examined using a portable energy-dispersive x-ray fluorescence (ED-XRF) device. The primary oxides of inorganic elements in the Khatatba Formation were investigated using the Bruker TRACER 5i Handheld XRF Analyzer. The data acquisition was performed using the ARTAX Spectra.7 calibration program. The samples were ground into a fine powder using a low trace element, hardened steel pulverizer. Pellets were subjected to a pressure of 40 tons and underwent triplicate analysis using low-energy X-ray fluorescence (XRF) for major elements and high-energy XRF for trace elements. The instrument required low-energy spectra signals below 13,000 raw counts per second (rcps), while high-energy spectra signals should range from around 1400 to 2000 rcps. The Limit of Detection (LDM) is the minimum concentration of an element in a particular sample that can be accurately measured under specified analytical conditions with a 95.4% confidence level. The principal elemental content of the 30 samples from the two wells was examined using energy dispersive x-ray fluorescence spectroscopy. The concentrations of all significant elements are expressed as weight percentages (wt %), whereas the concentrations of trace elements are expressed as parts per million (ppm).

3. Results and Discussion

3.1. Lithology Identification

The "Neutron porosity-Bulk density" cross plot was used and calibrated with Schlumberger cross plot chart to identify the main lithology for the studied formation in Matruh-5 and Matruh-6 wells. Each member was examined separately for better results. The density–neutron cross plots of the Lower and Upper Safa members in Matruh-5 and Matruh-6 wells show mixed lithology of sandstones, shale, siltstone, and carbonates was found in the Lower and Upper Safa members **(Fig.3)** Respectively.

3.2 Elemental Analysis (TOC and CaCO3)

The carbonate content shows strong fluctuations and appears to have a negative relationship with the TOC (**Fig. 4 and its tabulated data**). Within the Matruh-5 well, the Lower Safa samples have a comparatively elevated CaCO3 content, compared to an average of 6.48% in Upper Safa Member (**Figs. 4 A, E**). On the other hand, in Matruh-6 samples start with 2.6% carbonate content in the Lower Safa Member, which increases toward the Upper Safa to exceed 66%. The Upper Safa samples in Matruh-6 well are very rich in carbonates with an average of more than 20% compared to the Lower Safa Member, with an average of 15.76%. Overall, the samples demonstrate an inverse correlation between CaCO3 and TOC% (**Figs. 4 B, F**). The total organic carbon percentage (TOC wt %) (Measured in Laboratory) exhibits a moderate level and has a negative correlation with the calcium carbonate percentage (CaCO3%). This pattern aligns with the overall trend observed in all samples from the same well, which range from suboxic to oxic conditions. In **Figure 4**, Matruh-5 well crossplots illustrate shallow marine carbonate-rich environments with positive correlation between TOC and silica in Zahra Member; negative correlation between TOC and silica in Upper Safa and Lower Safa members (**Fig. 4C**). Moreover, Matruh-6 well crossplot (**Fig. 4D**) shows shallow marine carbonate-rich environments with positive correlation between TOC and silica in Zahra and Upper Safa members; negative correlation between TOC and silica in Lower Safa Member (**Bou Daher et al., 2015**). The possible depositional environment is shallow Marine environment. In Matruh-5 well, the $CaCO_3$ average content at Zahra Member reaches ~ 19%, while in the Upper Safa Member reaches an average of ~ 6.5% and in Lower Safa Member reaches an average of ~ 11.5%. However, in Matruh-6 well, $CaCO_3$ average content at Zahra Member reaches ~ 19%, while the Upper Safa Member reaches ~ 20% and Lower Safa Member reaches ~ 16%.

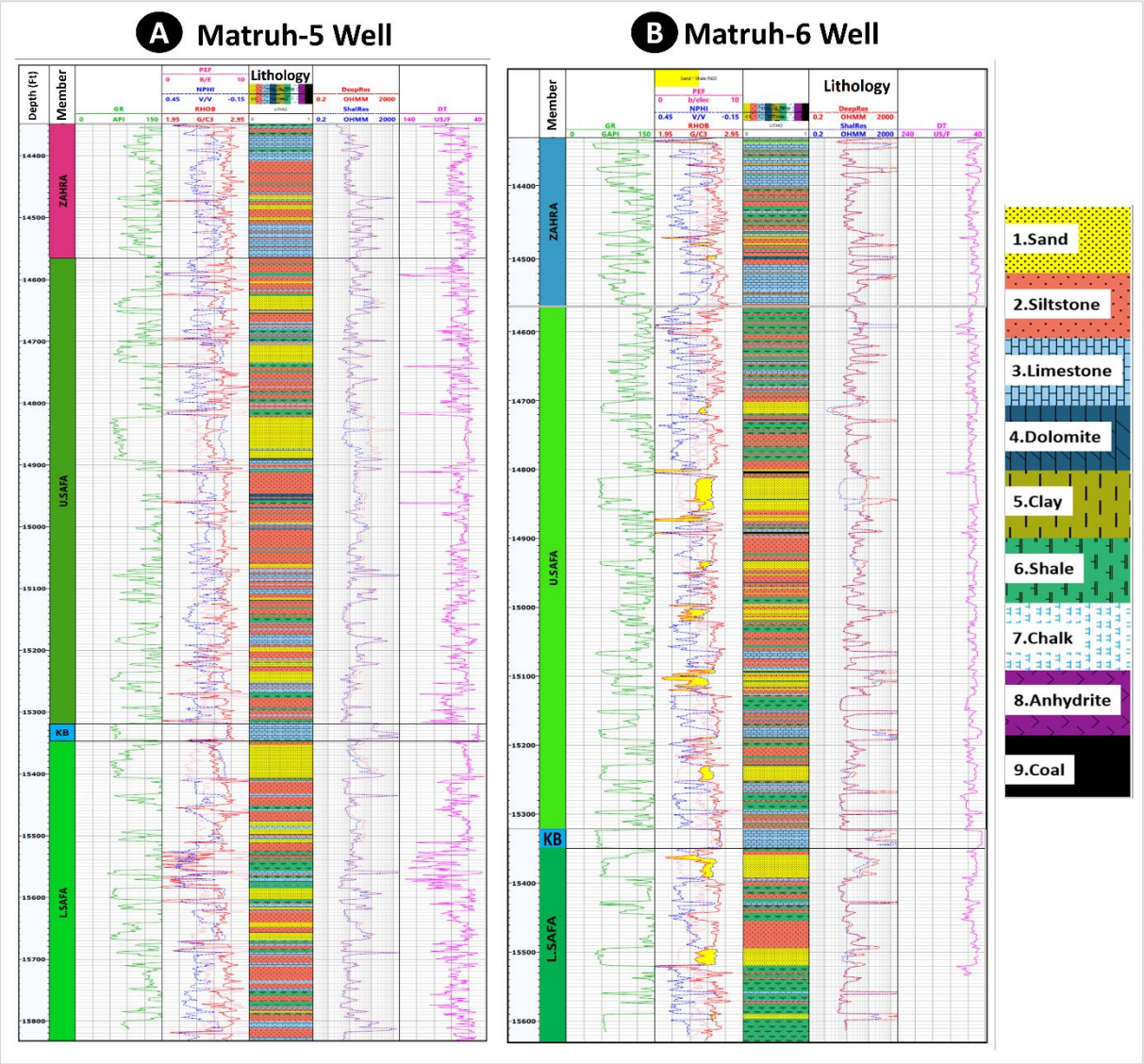

Fig. 3. Lithology Identification of the studied wells from wireline logs, for Khatatba Fm members, Zahra, Upper Safa, Kabrit (KB), and Lower Safa, where tack-1 represents the GR log, track-2 represents density-neutron logs, track-3 represents the interpreted lithology, track-4 represents the resistivity logs, and track-5 represents the DT-sonic log in both wells, (A): Matruh-5 well; (B): Matruh-6 well.

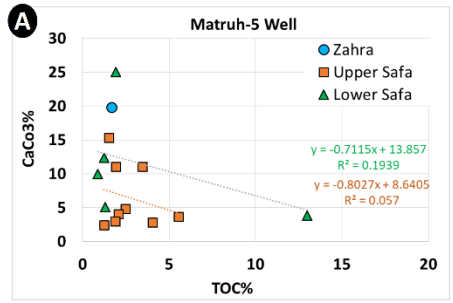

Well	Formation	Unit	Sample No.	Depth (ft)	Sample Type	Depth(m)	TOC%	CaCo3 (%)
Matruh-5	Khatatba Fm	Zahra	15	14516	Cuttings	4424	1.67	19.81
		Upper Safa	14	14576	Cuttings	4443	2.48	4.88
		Upper Safa	13	14606	Cuttings	4452	1.93	11.05
		Upper Safa	12	14746	Cuttings	4495	4.05	2.85
		Upper Safa	11	14816	Cuttings	4516	5.55	3.7
		Upper Safa	10	14946	Cuttings	4556	3.47	11.05
		Upper Safa	9	15056	Cuttings	4589	2.07	4.02
		Upper Safa	8	15086	Cuttings	4598	1.24	2.46
		Upper Safa	7	15216	Cuttings	4638	1.9	3
		Upper Safa	6	15316	Cuttings	4668	1.53	15.32
		Lower Safa	5	15426	Cuttings	4702	1.31	5.07
		Lower Safa	4	15686	Cuttings	4781	12.98	3.84
		Lower Safa	3	15716	Cuttings	4790	1.92	24.99
		Lower Safa	2	15846	Cuttings	4830	0.88	9.99
		Lower Safa	1	15886	Cuttings	4842	1.23	12.36

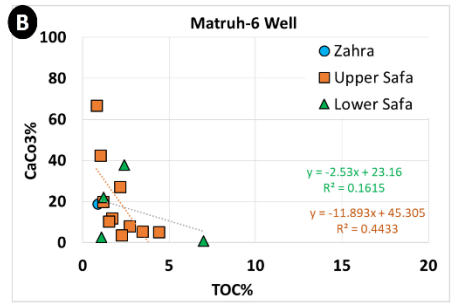

Well	Formation	Unit	Member	Depth (ft)	Cuttings	Depth(m)	TOC%	CaCo3 (%)
Matruh-6	Khatatba Fm	Zahra	15	14368	Cuttings	4379	0.86	18.78
		Zahra	14	14418	Cuttings	4395	1.71	11.77
		Zahra	13	14438	Cuttings	4401	1.52	10.39
		U.Safaa	12	14568	Cuttings	4440	1.03	42.42
		U.Safaa	11	14608	Cuttings	4453	4.42	5.06
		U.Safaa	10	14678	Cuttings	4474	2.17	27.08
		U.Safaa	9	14748	Cuttings	4495	2.73	7.93
		U.Safaa	8	14778	Cuttings	4504	2.27	3.47
		U.Safaa	7	15168	Cuttings	4623	1.18	19.81
		U.Safaa	6	15188	Cuttings	4629	0.8	66.77
		U.Safaa	5	15218	Cuttings	4638	3.44	5.39
		L.Safaa	4	15418	Cuttings	4699	1.22	21.99
		L.Safaa	3	15528	Cuttings	4733	6.99	0.79
		L.Safaa	2	15578	Cuttings	4748	1.08	2.6
		L.Safaa	1	15618	Cuttings	4760	2.41	37.66

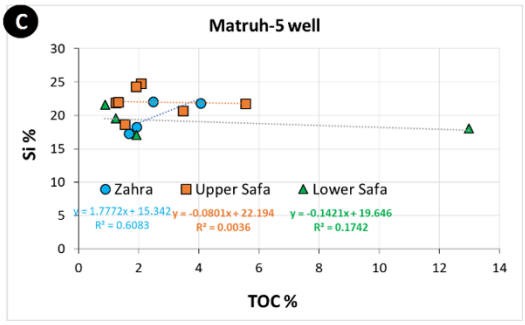

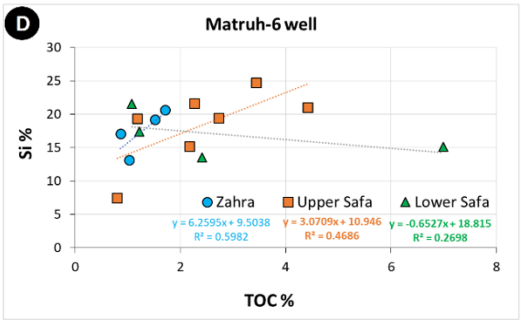

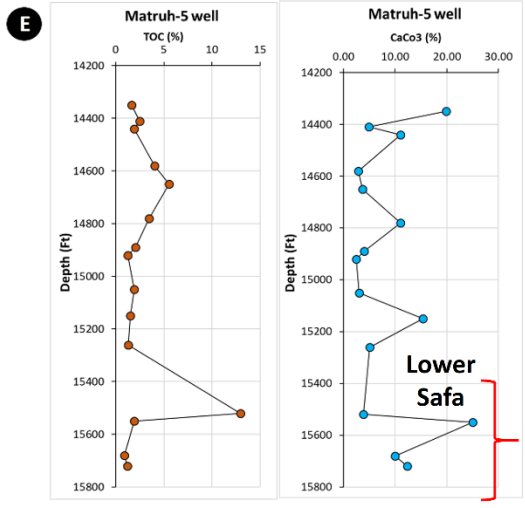

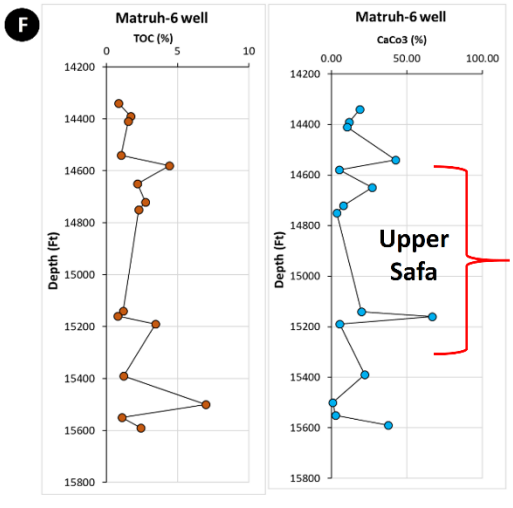

Fig. 4. (A, B). TOC % and $CaCO_3$ % Crossplot in Matruh-5 and Matruh-6 wells respectively. The tabulated data for Matruh-5 and Matruh-6 wells are on the right of the crossplots. (C): TOC% and CaCO3 % versus Depth in Matruh-5 well show elevation in carbonate content in Lower Safa Member. (D): TOC% and CaCO3 % versus Depth in Matruh-6 well, show elevation in carbonate content in Upper Safa Member. (C, D): Crossplot of TOC% versus Si% in Matruh-5 and Matruh-6 wells for Khatatba Fm Members; (E, F): Depth versus TOC%, CaCo3% for Matruh-5 and Matruh-6 wells.

Paleoclimate

The examined samples exhibit elevated K/Al and Si/Al ratios, indicating the prevalence of illite in the silicate mineral compositions found in the low carbonate deposits. This suggests a dry and warm climate (**Fig. 5**). Moreover, The Fe/Mn ratio is employed as an indicator of paleoclimatic conditions as well. Elevated ratios suggest warm and humid circumstances, whereas low ratios suggest hot and dry conditions (**Shang et al., 2022; Wang et al., 2020**).

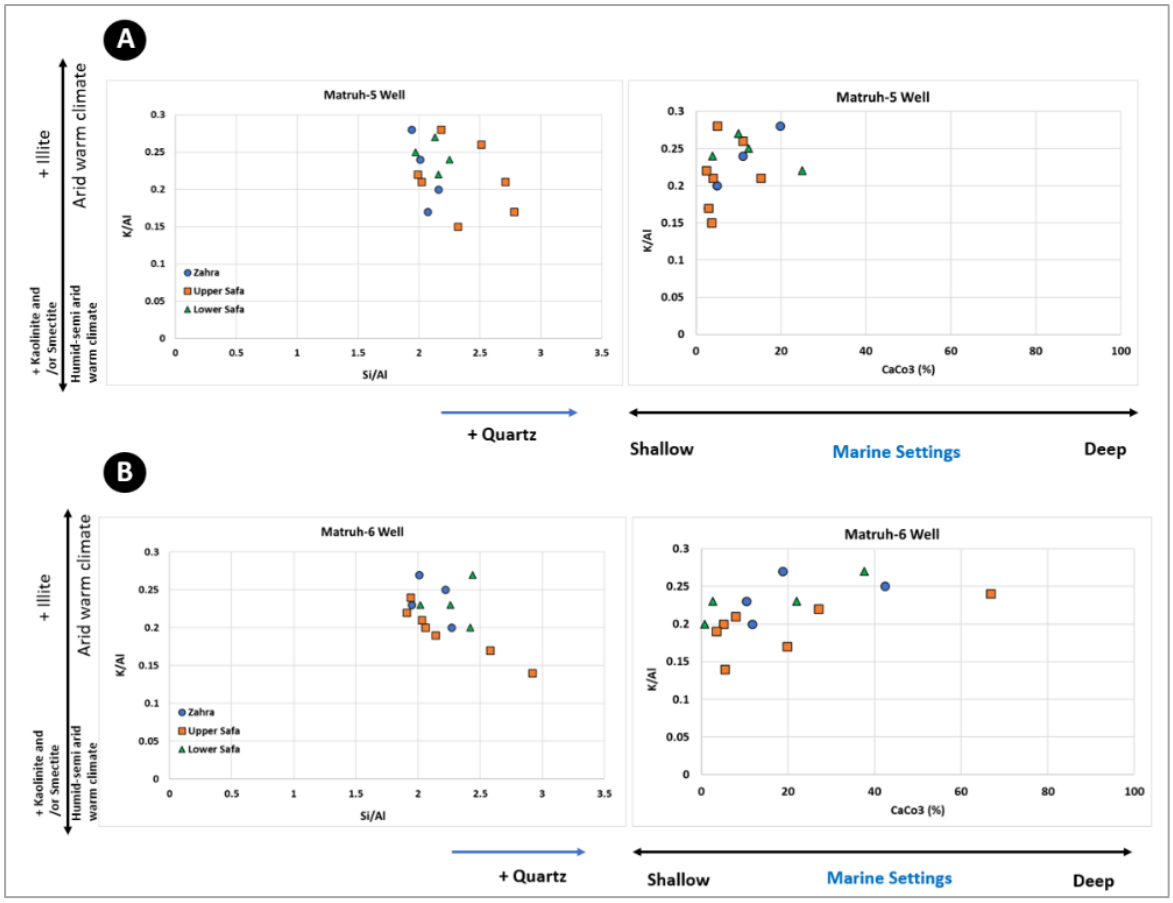

Fig. 5. The paleoclimate of Khataba Formation is determined using the K/Al versus Si/Al cross-plot, which suggests the presence of illite and indicates a semi-arid to arid warm climate. The depositional environment is interpreted from the cross-plot of CaCo3% versus K/Al ratio, which suggests a shallow marine environment (Aquit et al., 2016; Niebuhr, 2005).

In Matruh-5 well, the Fe/Mn ratios of the Upper Safa Member range from 31.6 to 72.27, with an average of 58.18. These ratios suggest a warm, semi-humid climate, as seen in **Figure 6A**. The Lower Safa Member exhibit comparatively elevated ratios (62.56 to 79.69) with an average 70.62 suggesting the development of more moist environmental conditions. Additionally, Zahra Member examined sample shows high value of Fe/Mn ratio reached 68.6. Yet, the majority of the Upper Safa Member in Matruh-5 well exhibit significantly lower Fe/Mn ratios as a result of the substantial increase in Mn concentrations, which rose from an average of 924.4 ppm in the Lower Safa Member to an average of 1362 ppm in the Upper Safa Member.

In Matruh-6 well, the Fe/Mn ratios the Upper Safa Member range from 37.61 to 96.14, with an average of 56.63. These ratios suggest a warm, semi-humid climate, as seen in Figure 6D. The Lower Safa Member exhibit comparatively elevated ratios (58.45 to 87.72) with an average 73.55 suggesting the emergence of more humid environmental conditions. Additionally, Zahra Member examined samples shows high value of Fe/Mn ratio reached (57.85-71.85 with an average 65.84). Yet, it is clear from the values that the majority of the Upper Safa Member in Matruh-6 well exhibit significantly lower Fe/Mn ratios than Zahra and Lower Safa member as a result of the substantial increase in Mn concentrations **(Fig 6, E),** which rose from an average of 871 ppm in the Lower Safa to an average of 1118 ppm in Zahra Member and an average of 1186.12 in the Upper Safa Member. The elevated levels of Mn are likely attributed to the less reducing (i.e., comparatively oxygen-rich) circumstances of these samples, which were conducive to the oxidation and subsequent formation of manganese oxides **(Calvert and Pedersen, 2007; Tribovillard et al., 2006).**

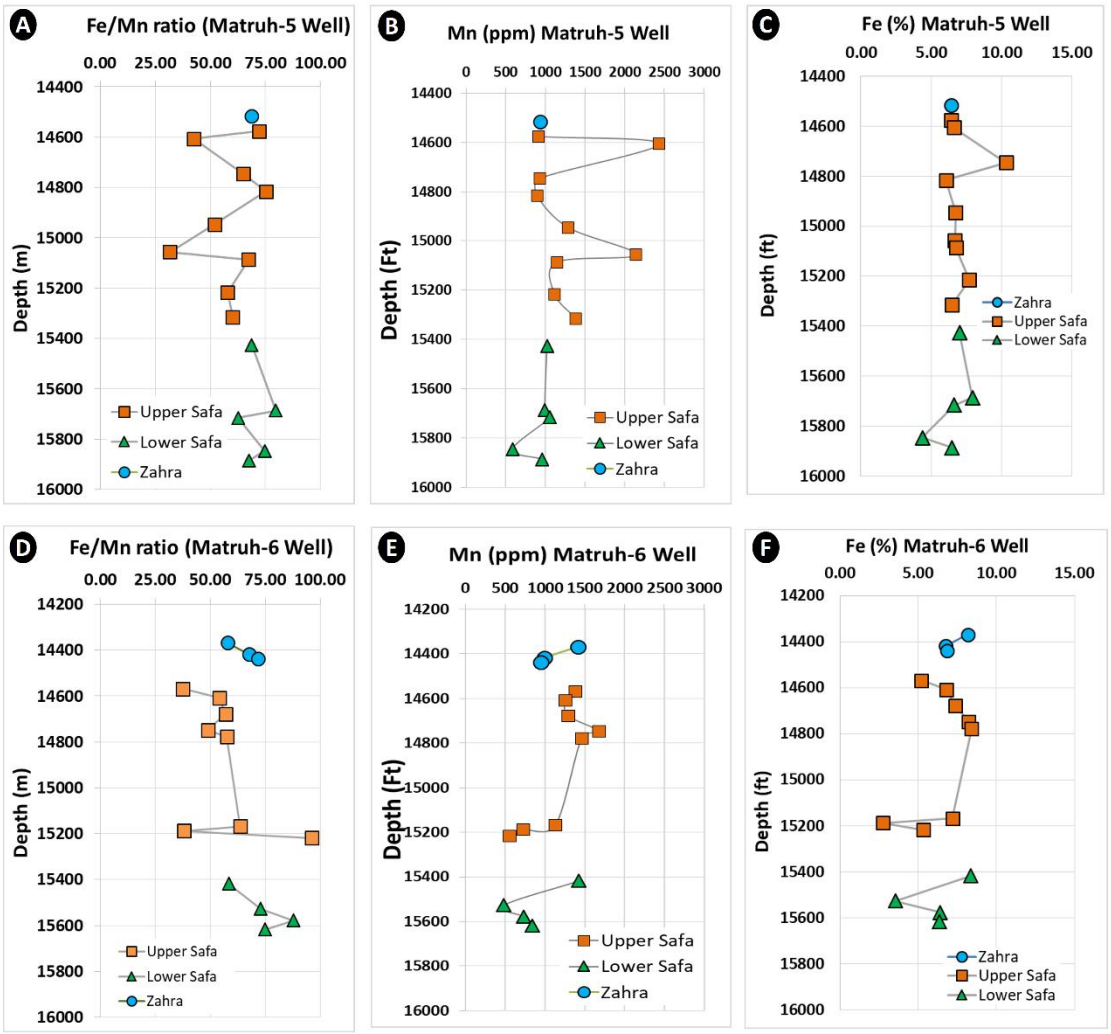

Fig. 6. Composite figure show (A, D): the Fe/Mn Ratio versus Depth, (B, E): Mn (ppm) concentration, (C, F): Fe% in Matruh-5 well and Matruh-6 well respectively.

Depositional Environment

The correlation between total organic carbon (TOC) and Iron (Fe) levels in a selected sample suggests that the environment in which the sample was deposited was rich in iron and had oxygen levels ranging from well-oxygenated to partially oxygenated. This is illustrated in (**Fig 7 C, D**). When there is enough detrital iron and increased burial of organic matter, the development of diagenetic pyrite will have a weak positive association with TOC because hydrogen sulfide (H_2S) does not occur at the interface between sediment and water (**Schultz, 2004**).

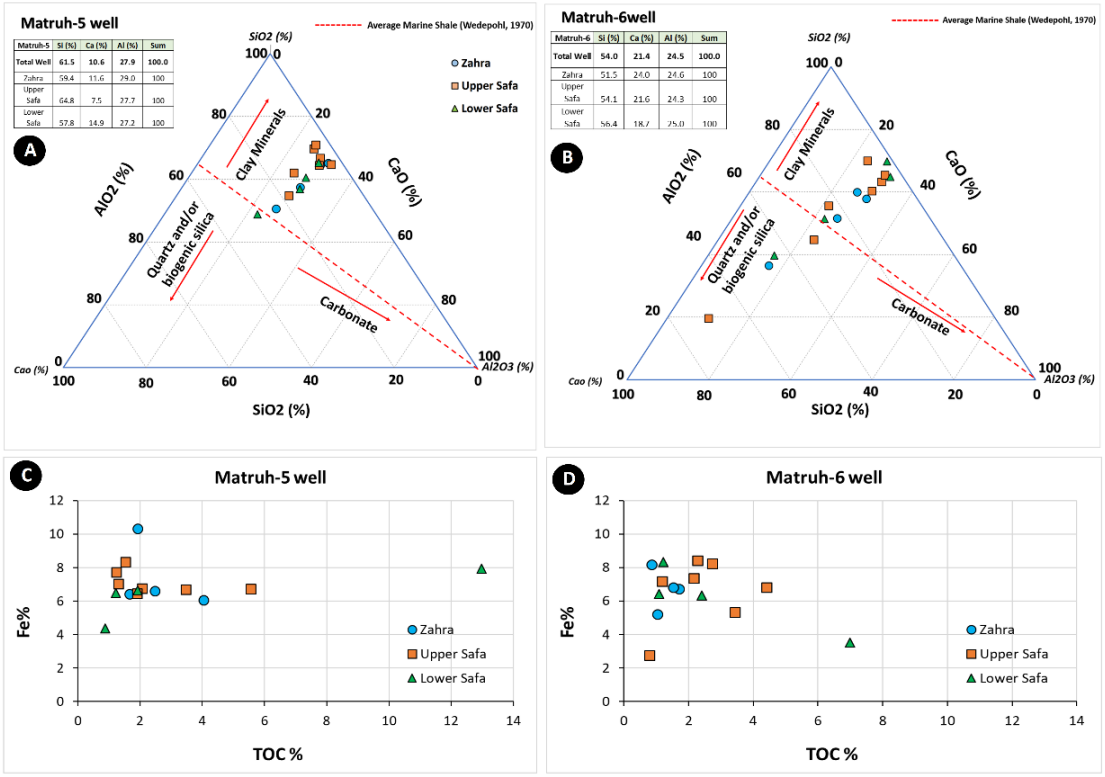

Fig. 7. A ternary diagram for the Matruh-5 and Matruh-6 wells, which uses SiO2-Al2O3-CaO to analyze the composition of shale/marlstone. This analysis assumes that shale is mostly made up of quartz, clay minerals, and carbonate, as described by (Brumsack, 1991). The crossplots of TOC% vs Fe% in Matruh-5 and Matruh-6 wells (C and D) suggest that the depositional habitat of these wells is a shallow marine environment with an abundance of iron, characterized by oxic to suboxic conditions.

The presence of a significant amounts of detrital elements suggests a period of regional sea regression, during which sediments are enriched with terrestrial elements such as Fe, Ti, K, and Mn **(Fig. 8).** The variations in the organic content suggest a marine environment that is quite close to the surface, where variations in the conditions of the water at the bottom are highly responsive to fluctuations in sea level.

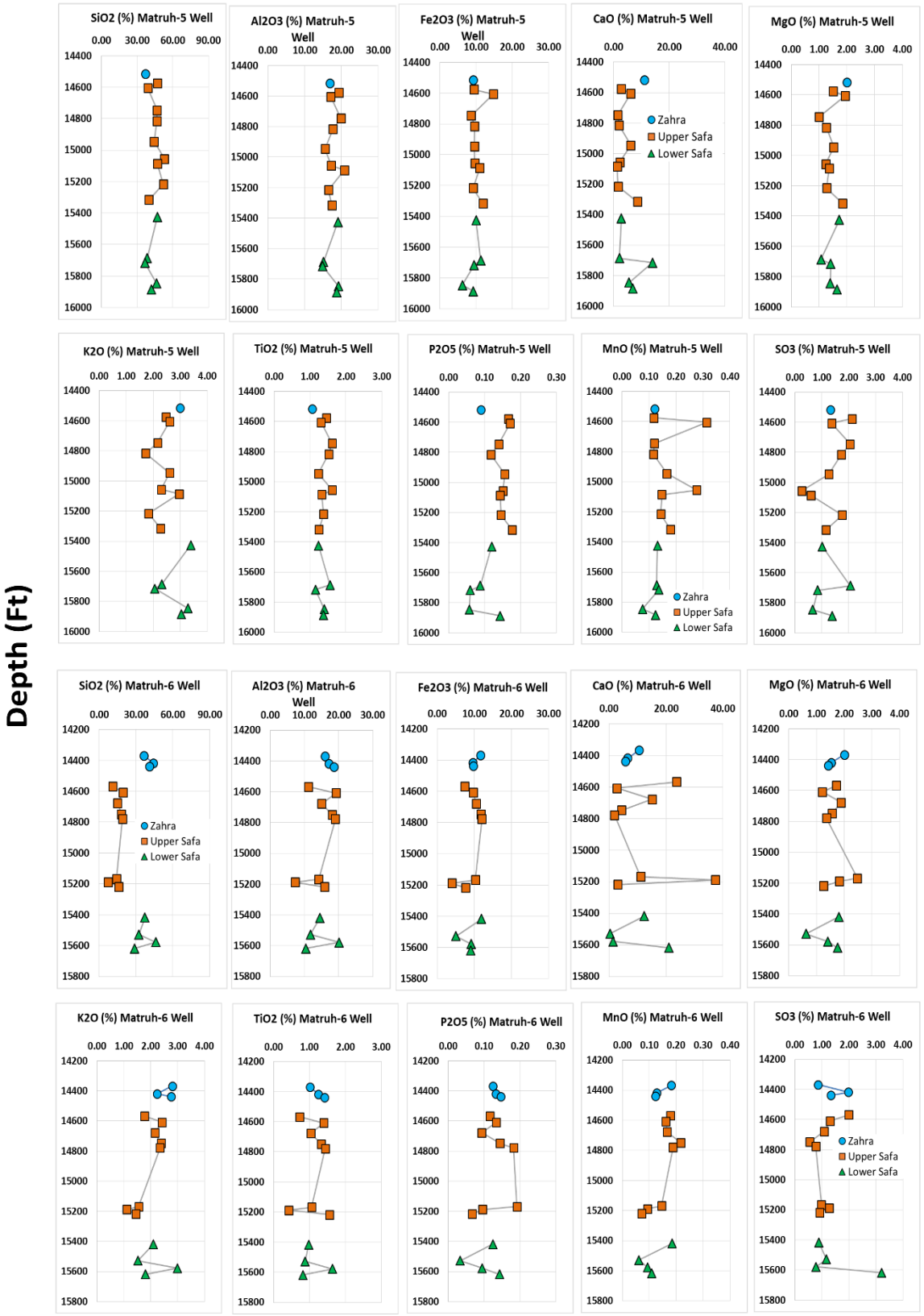

Fig. 8. Terrestrial Input of Khatatba Fm elemental data versus depth for Matruh-5 and Matruh-6 wells.

The Si/Al ratio indicates a change in the proportion of silicate minerals (such as clay and feldspar) to quartz. The Fe/Al ratios are frequently used as a measure of pyrite formation and redox conditions, employing the "Degree of Pyritization" (**Lyons et al., 2003; Wei et al., 2012**) as an indication. The K/Al ratio is used as a measure of clay mineral composition, where high values indicate an abundance of illite and so signify a dry and hot climate. In contrast, low levels suggest the existence of kaolinite/smectite combinations, which are linked to a warm environment that is either humid or semi-arid. The samples demonstrate increased K/Al and Si/Al ratios, suggesting the dominance of illite in the silicate mineral compositions present in the low carbonate deposits. This suggests a dry and warm climate. The P/Al Ratio is employed as an indicator of the paleo-environment. **März et al. (2008)** suggested that ratios greater than 0.4 indicate the presence of anoxic, non-sulfidic conditions. However, P/Al ratios for the tested samples in Matruh-5 and Matruh-6 wells did not exceed 0.01. This indicates that the conditions in these wells are within the range of oxic-suboxic conditions.

On the other hand, the V/Cr ratio is commonly employed in conjunction with Cr to assess and measure redox conditions in the diagenetic nitrate reduction zone **(Ferriday & Montenari, 2016; Wignall, 1994).** When V/Cr levels are higher than two, it suggests the presence of anoxia. On the other hand, values below two are regarded normal for oxic conditions (**Nagarajan et al., 2007; Schroder and Grotzinger, 2007).** Vanadium to chromium ratio levels below two are considered indicative of oxygen-rich environments (**Fig. 9 A, B**). Conversely, Cu/Zn ratios serve as markers of redox reactions, where high levels indicate reducing conditions and low values indicate oxidizing conditions (**Fig. 9 C, D**).

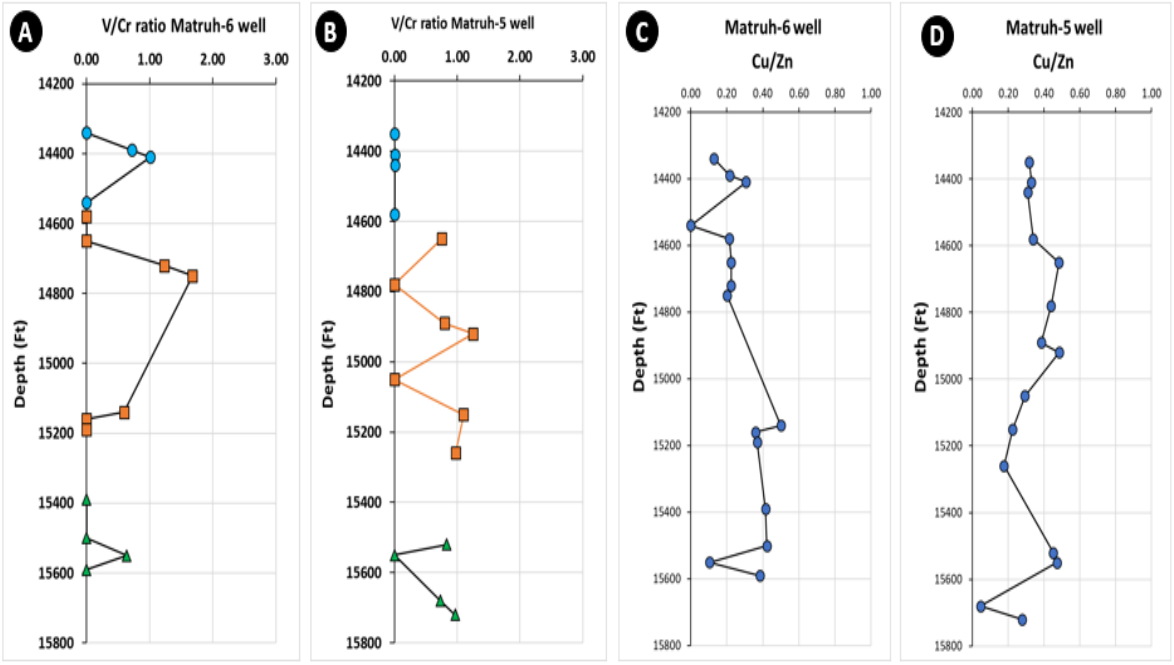

Fig. 9. Trace elements as paleoenvironmental indicators, (A) and (B) show V/Cr ratio values below two are thought to be characteristic for oxic conditions in Matruh-5 and Matruh-6 wells. (C) and (D): show Cu/Zn ratios used as redox indicators, where low values specifying oxidizing environments (Nagarajan et al., 2007).

Table 1. Major (wt %) and trace (ppm) element compositions of Khatatba Fm members in Matruh-5 well.

Well	Matruh-5	Matruh-5	Matruh-5	Matruh-5	Matruh-5	Matruh-5	Matruh-5	Matruh-5	Matruh-5	Matruh-5	Matruh-5	Matruh-5	Matruh-5	Matruh-5	Matruh-5
Unit	Zahra	Upper Safa	Upper Safa	Upper Safa	Upper Safa	Upper Safa	Upper Safa	Upper Safa	Upper Safa	Upper Safa	Lower Safa	Lower Safa	Lower Safa	Lower Safa	Lower Safa
Sample No.	15	14	13	12	11	10	9	8	7	6	5	4	3	2	1
Depth (ft)	14516	14576	14606	14746	14816	14946	15056	15086	15216	15316	15426	15686	15716	15846	15886
Sample Type	Cuttings	Cuttings	Cuttings	Cuttings	Cuttings	Cuttings	Cuttings	Cuttings	Cuttings	Cuttings	Cuttings	Cuttings	Cuttings	Cuttings	Cuttings
Depth(m)	4424	4443	4452	4495	4516	4556	4589	4598	4638	4668	4702	4781	4790	4830	4842
SiO2%	36.97	47.08	39.04	46.69	46.52	44.26	52.95	46.91	51.98	39.85	46.95	38.51	36.43	46.16	41.84
Al2O3%	16.85	19.28	17.12	19.88	17.70	15.57	17.23	20.80	16.49	17.39	19.05	15.15	14.88	19.14	18.72
Fe2O3%	9.17	9.43	14.76	8.66	9.63	9.56	9.68	11.02	9.22	11.92	10.03	11.34	9.47	6.26	9.27
FeO%	8.25	8.49	13.28	7.79	8.67	8.60	8.71	9.92	8.30	10.73	9.03	10.20	8.52	5.63	8.34
CaO%	11.09	2.73	6.19	1.59	2.07	6.18	2.25	1.37	1.68	8.58	2.84	2.15	13.99	5.59	6.92
MgO%	2.00	1.52	1.95	0.99	1.27	1.53	1.24	1.37	1.28	1.85	1.73	1.08	1.43	1.41	1.64
K2O%	3.00	2.47	2.61	2.16	1.72	2.60	2.30	2.96	1.83	2.28	3.40	2.32	2.06	3.29	3.04
Na2O%	0.00	0.73	0.00	0.55	0.65	0.66	0.87	0.58	0.50	0.00	0.55	0.00	0.00	0.44	0.59
TiO2%	1.06	1.45	1.31	1.61	1.52	1.23	1.62	1.33	1.38	1.25	1.24	1.56	1.16	1.40	1.38
MnO%	0.12	0.12	0.31	0.12	0.12	0.17	0.28	0.15	0.14	0.18	0.13	0.13	0.14	0.08	0.12
P2O5%	0.09	0.17	0.17	0.14	0.12	0.16	0.15	0.14	0.15	0.18	0.12	0.09	0.06	0.06	0.14
SO3%	1.33	2.12	1.36	2.05	1.72	1.26	0.26	0.59	1.76	1.15	1.02	2.06	0.85	0.67	1.39
LIO%	17.14	11.71	16.45	14.56	22.92	14.67	18.19	13.06	11.25	19.38	13.22	22.16	20.31	13.79	15.85
Pb (ppm)	0	30	0	29	0	0	22	0	30	29	0	0	0	0	27
Zn (ppm)	110	112	84	106	60	66	78	68	68	120	153	73	55	557	97
Th (ppm)	4	5	3	4	3	5	5	7	5	5	7	5	3	6	7
Ni (ppm)	37	32	34	32	28	29	27	26	30	31	31	28	23	33	36
Co (ppm)	36	27	50	27	30	33	31	35	29	42	33	34	37	21	33
Cr (ppm)	156	176	165	160	147	120	144	137	179	139	125	146	106	125	134
Rb (ppm)	76	56	59	57	39	75	65	92	57	68	110	53	56	96	84
Nb (ppm)	21	27	22	36	28	30	28	29	28	27	32	39	29	39	39
Zr (ppm)	249	383	300	423	469	387	420	322	423	316	308	375	300	390	356
Y (ppm)	33	46	35	37	37	42	39	42	37	38	33	37	36	41	41
Sr (ppm)	1640	176	195	132	117	163	146	155	131	253	198	139	278	579	217
V (ppm)	0	123	117	87	111	0	115	172	0	153	122	122	0	92	130
Mo (ppm)	17	24	19	27	24	24	24	19	24	19	21	19	19	22	24
Ba (ppm)	148	297	227	233	161	356	346	305	358	220	250	443	266	0	179
U (ppm)	0	0	0	0	0	0	0	15	0	0	0	0	0	0	13
Cu (ppm)	35	37	26	36	29	29	30	33	20	27	27	33	26	26	27
Ga (ppm)	33	30	29	31	26	27	21	38	22	35	35	28	25	40	37
As (ppm)	12	14	12	13	9	11	9	12	11	7	9	6	7	9	10
K2O/Al2O3	0.18	0.13	0.15	0.11	0.10	0.17	0.13	0.14	0.11	0.13	0.18	0.15	0.14	0.17	0.16
Al2O3/TiO2	15.85	13.26	13.05	12.31	11.61	12.64	10.61	15.66	11.97	13.88	15.33	9.73	12.87	13.69	13.61
SiO2/Al2O3	2.19	2.44	2.28	2.35	2.63	2.84	3.07	2.26	3.15	2.29	2.46	2.54	2.45	2.41	2.23
D*	0.7	0.6	0.7	0.7	0.7	0.6	0.6	0.7	0.6	0.7	0.6	0.6	0.7	0.7	0.7
CIA	54.5	76.5	66.1	82.2	79.9	62.2	76.1	80.9	80.4	61.6	73.7	77.2	48.1	67.2	64.0
CIW	60.3	84.8	73.5	90.3	86.7	69.5	84.7	91.4	88.3	67.0	84.9	87.6	51.5	76.0	71.4
ICV	1.5	0.9	1.5	0.7	0.9	1.3	1.0	0.8	0.9	1.4	1.0	1.1	1.8	0.9	1.2

LOI: loss on ignition
D*: Al2O3/(Al2O3+MnO+FeOtot); (**Machour *et al.*, 1994**)

Table 2. Major (wt %) and trace (ppm) element compositions of Khatatba Fm members in Matruh-6 well.

Well	Matruh-6	Matruh-6	Matruh-6	Matruh-6	Matruh-6	Matruh-6	Matruh-6	Matruh-6	Matruh-6	Matruh-6	Matruh-6	Matruh-6	Matruh-6	Matruh-6	Matruh-6
Unit	Zahra	Zahra	Zahra	Upper Safa	Upper Safa	Upper Safa	Upper Safa	Upper Safa	Upper Safa	Upper Safa	Upper Safa	Lower Safa	Lower Safa	Lower Safa	Lower Safa
Member	15	14	13	12	11	10	9	8	7	6	5	4	3	2	1
Depth (ft)	14368	14418	14438	14568	14608	14678	14748	14778	15168	15188	15218	15418	15528	15578	15618
Sample Type	Cuttings	Cuttings	Cuttings	Cuttings	Cuttings	Cuttings	Cuttings	Cuttings	Cuttings	Cuttings	Cuttings	Cuttings	Cuttings	Cuttings	Cuttings
Depth(m)	4379	4395	4401	4440	4453	4474	4495	4504	4623	4629	4638	4699	4733	4748	4760
SiO2%	36.51	44.12	41.06	28.19	44.95	32.51	41.62	46.26	41.43	16.00	52.89	37.27	32.30	46.12	28.97
Al2O3%	16.06	17.16	18.64	11.19	19.27	15.06	18.15	19.06	14.20	7.29	15.99	14.57	11.78	20.20	10.49
Fe2O3%	11.68	9.63	9.75	7.45	9.74	10.53	11.76	12.03	10.27	3.94	7.63	11.93	5.03	9.17	9.05
FeO%	10.51	8.66	8.77	6.70	8.76	9.48	10.58	10.83	9.24	3.55	6.86	10.73	4.53	8.25	8.15
CaO%	10.51	6.59	5.82	23.74	2.83	15.16	4.44	1.94	11.09	37.37	3.02	12.31	0.44	1.45	21.08
MgO%	2.01	1.54	1.42	1.71	1.21	1.89	1.56	1.36	2.48	1.82	1.26	1.80	0.62	1.40	1.76
K2O%	2.80	2.24	2.77	1.78	2.43	2.16	2.39	2.35	1.55	1.11	1.44	2.10	1.52	2.99	1.80
Na2O%	0.00	0.82	0.56	0.00	0.00	0.00	0.00	0.68	0.52	0.00	0.72	0.00	0.00	0.40	0.00
TiO2%	1.02	1.25	1.42	0.73	1.40	1.04	1.34	1.44	1.06	0.43	1.56	0.98	0.88	1.64	0.82
MnO%	0.18	0.13	0.12	0.18	0.16	0.17	0.22	0.19	0.15	0.09	0.07	0.18	0.06	0.09	0.11
P2O5%	0.12	0.13	0.15	0.12	0.13	0.09	0.14	0.18	0.19	0.10	0.07	0.12	0.03	0.09	0.14
SO3%	0.85	1.99	1.33	2.00	1.31	1.08	0.55	0.78	0.98	1.26	0.92	0.89	1.17	0.78	3.21
LIO%	19.01	14.08	13.67	38.35	29.83	22.34	15.94	13.40	16.72	31.61	14.43	14.37	15.53	12.92	23.41
Pb (ppm)	0	30	29	0	0	0	0	0	0	0	0	0	0	0	0
Zn (ppm)	116	79	62	45	98	107	94	124	54	39	65	53	90	210	52
Th (ppm)	4	4	5	3	6	4	6	5	3	2	4	4	3	7	2
Ni (ppm)	32	31	28	20	28	34	43	29	25	13	25	35	33	30	28
Co (ppm)	45	35	32	32	31	43	39	37	40	19	24	45	11	28	39
Cr (ppm)	143	149	111	112	131	130	128	121	192	0	111	182	120	146	168
Rb (ppm)	71	57	66	40	65	58	68	62	46	30	38	66	62	94	46
Nb (ppm)	21	25	24	13	32	23	28	29	21	8	40	20	25	49	16
Zr (ppm)	229	326	314	215	334	259	331	367	299	107	528	264	347	512	208
Y (ppm)	35	34	39	35	36	32	42	40	30	16	38	32	31	42	27
Sr (ppm)	220	177	197	362	157	314	182	135	201	549	175	246	124	205	442
V (ppm)	0	107	112	0	0	0	158	203	114	0	0	0	0	93	0
Mo (ppm)	18	21	21	12	22	18	22	20	20	10	34	27	20	28	16
Ba (ppm)	146	207	284	258	392	620	529	443	354	180	287	152	519	0	286
U (ppm)	0	0	0	0	0	0	0	0	0	0	0	0	0	0	0
Cu (ppm)	15	17	19	0	21	24	21	25	27	14	24	22	38	22	20
Ga (ppm)	25	27	28	16	23	26	28	31	18	8	23	21	26	41	14
As (ppm)	7	8	9	7	11	8	11	13	7	0	9	7	6	7	6
K2O/Al2O3	0.17	0.13	0.15	0.16	0.13	0.14	0.13	0.12	0.11	0.15	0.09	0.14	0.13	0.15	0.17
Al2O3/TiO2	15.71	13.69	13.12	15.44	13.80	14.50	13.59	13.20	13.39	16.97	10.25	14.88	13.36	12.31	12.79
SiO2/Al2O3	2.27	2.57	2.20	2.52	2.33	2.16	2.29	2.43	2.92	2.19	3.31	2.56	2.74	2.28	2.76
D*	0.6	0.7	0.7	0.6	0.7	0.6	0.6	0.7	0.8	0.5	0.6	0.8	0.6	0.7	1.0
CIA	54.7	64.0	67.1	30.5	78.6	46.5	72.7	79.3	51.9	15.9	75.5	50.3	85.7	80.7	31.4
CIW	60.4	69.9	74.5	32.0	87.2	49.8	80.4	87.9	55.0	16.3	81.1	54.2	96.4	91.6	33.2
ICV	1.7	1.2	1.1	3.1	0.9	2.0	1.1	1.0	1.8	6.1	0.9	1.9	0.7	0.8	3.2

LOI: loss on ignition
D*: Al2O3/(Al2O3+MnO+FeOtot); (**Machour *et al.*, 1994**)

Table 3. Elemental ratios of Khatatba Fm members in Matruh-5 and Matruh-6 wells.

Well	Unit	Sample No.	Depth (ft)	Sample Type	Depth(m)	Fe/Al	Mn/S	Si/Al	Mg/Ca	Ti/Al	P/Al	Mg/Ca	Cr/Al	Fe/Mn	K/Al	Sr/Cu	K/Rb	Sr/Ca	Rb/Sr
Matruh-5	Zahra	15	14516	Cuttings	4424	0.72	0.18	1.94	0.15	0.07	0.004	0.15	0.002	68.61	0.28	46.86	327	0.021	0.05
Matruh-5	Upper Safa	14	14576	Cuttings	4443	0.647	0.11	2.16	0.47	0.09	0.007	0.47	0.002	72.27	0.20	4.76	366	0.009	0.32
Matruh-5	Upper Safa	13	14606	Cuttings	4452	1.14	0.45	2.01	0.27	0.09	0.008	0.27	0.002	42.37	0.24	7.50	367	0.004	0.30
Matruh-5	Upper Safa	12	14746	Cuttings	4495	0.576	0.11	2.07	0.53	0.09	0.006	0.53	0.002	65.07	0.17	3.67	315	0.012	0.43
Matruh-5	Upper Safa	11	14816	Cuttings	4516	0.72	0.13	2.32	0.52	0.10	0.005	0.52	0.002	75.21	0.15	4.03	367	0.008	0.33
Matruh-5	Upper Safa	10	14946	Cuttings	4556	0.811	0.26	2.51	0.21	0.09	0.008	0.21	0.001	51.86	0.26	5.62	288	0.004	0.46
Matruh-5	Upper Safa	9	15056	Cuttings	4589	0.742	2.03	2.71	0.47	0.11	0.007	0.47	0.002	31.57	0.21	4.87	294	0.009	0.45
Matruh-5	Upper Safa	8	15086	Cuttings	4598	0.701	0.48	1.99	0.84	0.07	0.006	0.84	0.001	67.29	0.22	4.70	267	0.016	0.59
Matruh-5	Upper Safa	7	15216	Cuttings	4638	0.739	0.16	2.78	0.64	0.09	0.007	0.64	0.002	57.78	0.17	6.55	266	0.011	0.44
Matruh-5	Upper Safa	6	15316	Cuttings	4668	0.906	0.30	2.02	0.18	0.08	0.008	0.18	0.002	60.16	0.21	9.37	278	0.004	0.27
Matruh-5	Lower Safa	5	15426	Cuttings	4702	0.696	0.25	2.18	0.51	0.07	0.005	0.51	0.001	68.79	0.28	7.33	256	0.010	0.56
Matruh-5	Lower Safa	4	15686	Cuttings	4781	0.989	0.12	2.25	0.42	0.12	0.005	0.42	0.002	79.69	0.24	4.21	363	0.009	0.38
Matruh-5	Lower Safa	3	15716	Cuttings	4790	0.842	0.31	2.16	0.09	0.09	0.003	0.09	0.001	62.56	0.22	10.69	306	0.003	0.20
Matruh-5	Lower Safa	2	15846	Cuttings	4830	0.432	0.22	2.13	0.21	0.08	0.002	0.21	0.001	74.68	0.27	22.27	285	0.014	0.17
Matruh-5	Lower Safa	1	15886	Cuttings	4842	0.654	0.17	1.97	0.20	0.08	0.006	0.20	0.001	67.39	0.25	8.04	300	0.004	0.39
Well	**Unit**	**Member**	**Depth (ft)**	**Sample Type**	**Depth(m)**	**Fe/Al**	**Mn/S**	**Si/Al ratio**	**Mg/Ca**	**Ti/Al**	**P/Al**	**Mg/Ca**	**Cr/Al**	**Fe/Mn**	**K/Al**	**Sr/Cu**	**K/Rb**	**Sr/Ca**	**Rb/Sr**
Matruh-6	Zahra	15	14368	Cuttings	4379	0.961	0.41	2.01	0.16	0.07	0.006	0.16	0.002	57.85	0.27	14.67	408	0.003	0.26
Matruh-6	Zahra	14	14418	Cuttings	4395	0.741	0.12	2.27	0.20	0.08	0.006	0.20	0.002	67.82	0.20	10.41	282	0.004	0.37
Matruh-6	Zahra	13	14438	Cuttings	4401	0.691	0.18	1.95	0.21	0.09	0.006	0.21	0.001	71.85	0.23	10.37	574	0.005	0.20
Matruh-6	U.Safaa	12	14568	Cuttings	4440	0.879	0.17	2.22	0.06	0.07	0.009	0.06	0.002	37.61	0.25	0.00	227	0.002	0.18
Matruh-6	U.Safaa	11	14608	Cuttings	4453	0.668	0.24	2.06	0.36	0.08	0.006	0.36	0.001	54.15	0.20	7.48	347	0.008	0.37
Matruh-6	U.Safaa	10	14678	Cuttings	4474	0.924	0.30	1.91	0.11	0.08	0.005	0.11	0.002	56.98	0.22	13.08	263	0.003	0.22
Matruh-6	U.Safaa	9	14748	Cuttings	4495	0.856	0.76	2.03	0.30	0.08	0.007	0.30	0.001	48.87	0.21	8.67	320	0.006	0.34
Matruh-6	U.Safaa	8	14778	Cuttings	4504	0.834	0.47	2.14	0.59	0.09	0.008	0.59	0.001	57.59	0.19	5.40	424	0.010	0.34
Matruh-6	U.Safaa	7	15168	Cuttings	4623	0.956	0.29	2.58	0.19	0.08	0.011	0.19	0.003	63.59	0.17	7.44	430	0.003	0.15
Matruh-6	U.Safaa	6	15188	Cuttings	4629	0.714	0.14	1.94	0.04	0.07	0.011	0.04	0.000	38.07	0.24	39.21	242	0.002	0.07
Matruh-6	U.Safaa	5	15218	Cuttings	4638	0.631	0.15	2.92	0.35	0.11	0.003	0.35	0.001	96.14	0.14	7.29	182	0.008	0.38
Matruh-6	L.Safaa	4	15418	Cuttings	4699	1.081	0.40	2.26	0.12	0.08	0.007	0.12	0.002	58.45	0.23	11.18	281	0.003	0.25
Matruh-6	L.Safaa	3	15528	Cuttings	4733	0.565	0.10	2.42	1.17	0.08	0.002	1.17	0.002	73.02	0.20	3.26	135	0.039	0.76
Matruh-6	L.Safaa	2	15578	Cuttings	4748	0.6	0.24	2.02	0.82	0.09	0.004	0.82	0.001	87.72	0.23	9.32	540	0.020	0.22
Matruh-6	L.Safaa	1	15618	Cuttings	4760	1.141	0.07	2.44	0.07	0.09	0.011	0.07	0.003	75.03	0.27	22.10	196	0.003	0.17

Table 4 demonstrates that the increase in the silica can be linked to a higher amount of terrigenous material and/or biogenic processes, such as enhanced biomineralization and sedimentation of siliceous skeletons and shells **(Calvert and Pedersen, 2007).** Higher levels of Al_2O_3 suggest significant weathering and greater sediment maturity, which can be recognized to the deposition of clay minerals from the water column. In addition, increased concentrations of K_2O suggest the presence of greater quantities of illite in a sediment. This is because illite is commonly formed by the introduction of K+ to kaolinite **(Wei et al., 2003).**

Table 4. Average major element characteristic of the Khatatba Fm in Matruh-5 and Matruh-6 wells.

	MgO wt%	Al2O3 wt%	SiO2 wt%	K2O wt%	MnO wt%	Fe2O3 wt%	Well Name
Min	0.60	7.87	17.03	1.43	0.06	4.38	Matruh-5
Max	1.21	11.01	24.75	2.82	0.24	10.32	
Average	0.90	9.36	20.64	2.11	0.12	6.97	
St.Dev	0.18	0.90	2.33	0.41	0.05	1.25	
Min	0.37	3.86	7.48	0.92	0.05	2.76	Matruh-6
Max	1.49	10.69	24.72	2.48	0.17	8.41	
Average	0.96	8.08	17.77	1.74	0.11	6.51	
St.Dev	0.25	1.91	4.19	0.44	0.04	1.64	

Terrestrial Influx

Titanium (Ti) is regarded as a more reliable indicator of the terrestrial influx compared to Aluminium (Al), because the overall (Al) concentrations can be influenced by authigenic or biogenic sources **(Wei et al., 2003).** According to **Burgan et al. (2008)**, strong positive correlation between Al_2O_3% and K_2O% is suggested to indicate their detrital origin. However, negative correlations of Ti with Al indicate no association with the aluminosilicate fraction, which occurs in Matruh-5 well and is not the case in the Matruh-6 well, which shows strong positive correlations of Ti with Al in Lower and Upper Safa members **(Fig 10, B)** indicating their association with the alumosilicate fraction **(Burgan et al., 2008).** Moreover, the

sedimentary rocks were classified and differentiated based on their chemical composition using the log (SiO_2/Al_2O_3) vs log (Fe_2O_3/K_2O) scheme developed by **Herron (1988).** The shales found in the Upper and Lower Safa members classed as belonging to the "Shale" and “Wacke” category (**Figs. 10C, F**).

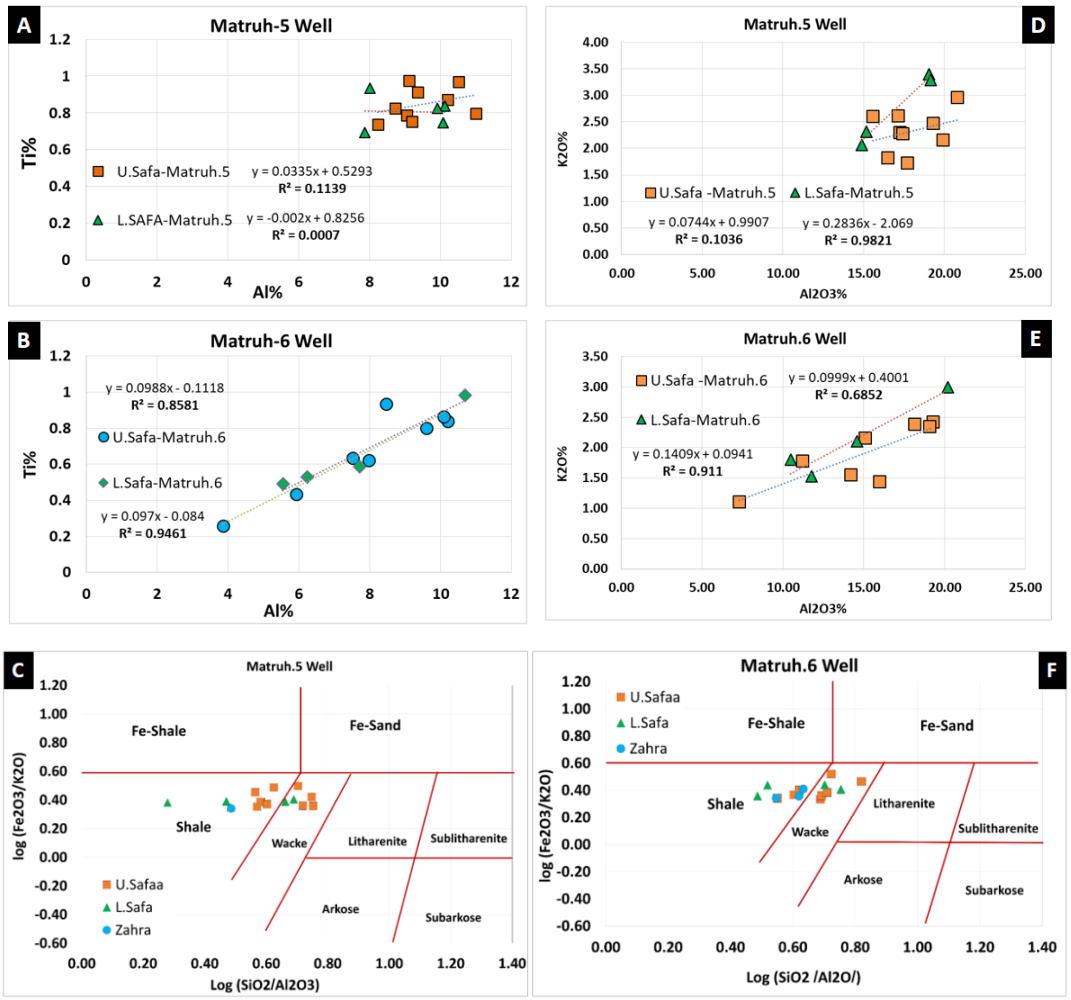

Fig. 10. Composite plot represents, (A): Al% versus Ti% crossplot shows weak correlation in Matruh-5 well. (B): Strong positive correlation between Al% versus Ti% in Matruh-6 well indicate their association with the alumosilicate fraction according to (Burgan et al., 2008). (D): In Matruh-5 shows week correlation in Upper Safa Member and strong correlation in Lower Safa Member. (E): Matruh-6 wells, crossplot shows strong positive correlation in Upper and Lower Safa members. (C) and (F) crossplots of log (SiO_2/Al_2O_3) ratio versus log (Fe_2O_3/K_2O) shows the geochemical classification of shale in the **studied siliciclastic sediments of the Khatatba Formation, the Matruh Basin, according to Herron (1988).**

The Index of compositional variation (ICV)

The compositional variation index refers to a measure of the degree of variation in a composition. The ICV and K_2O/Al_2O_3 values are commonly utilized alongside the weathering indices (chemical index of alteration “CIA” and chemical index of weathering “CIW”) (Tables 1, 2) to assess the degree of weathering, the level of recycling, and the maturity of sediments **(Barbera et al., 2006; Cullers and Podkovyrov, 2000; Okunlola et al., 2009).** Immature shales can have ICV values exceeding 1 due to a substantial influx of non-clay minerals such plagioclase, K-feldspar, amphiboles,

and pyroxenes. These minerals are commonly found in areas with active tectonism and/or in deposits formed during the initial cycle of erosion and sedimentation (syn-rift deposits) **(Campos Alvarez and Roser, 2007; Cox et al., 1995; Cullers and Podkovyrov, 2000).** Thus, the ICV values are utilized in conjunction with the K_2O/Al_2O_3 ratio to determine the relative abundance of alkali-feldspar, plagioclase, and clay minerals in sediments. Afterward, the aforementioned method, as explained by **Cox et al. (1995)**, is employed to approximate the initial mineral composition and the degree of maturity of ancient mud rocks. The ICV, CIA, and CIW are calculated using the following equations:

ICV = [(CaO + K_2O + Na_2O + Fe_2O_3 (t) + MgO + MnO + TiO_2)/Al_2O_3] **(Cox et al., 1995)**

CIA: Al2O3/ (Al2O3 + Na2O + CaO* + K2O) * 100; **(Nesbitt and Young, 1982)**

CIW: Al2O3/ (Al2O3 + Na2O + CaO*) * 100; **(Harnois, 1988).**

A K_2O/Al_2O_3 ratio of 0.5 indicates a significant presence of feldspar relative to the concentration of clay minerals, which is a distinguishing feature of immature sediments. Values less than 0.4 indicate a scarcity of feldspar in the original shale and suggest strata that have experienced substantial maturation (**Cox et al., 1995; Cullers and Podkovyrov, 2000)**. In table 4 below, the K_2O/Al_2O_3 elemental ratio in Matruh-5 and Matruh-6 wells are below 0.4, which suggest sediments maturation. Additionally, The K_2O/Al_2O_3 ratios are also utilized to deduce chemical weathering, wherein intense weathering converts K_2O-rich minerals (such as feldspars) into aluminosilicate-rich clay minerals (**Cox et al., 1995**). Therefore, K_2O/Al_2O_3 ratios greater than 0.5 indicate a larger presence of clay minerals and intense weathering, whereas ratios below 0.5 suggest a higher proportion of alkali feldspar and minimal weathering. In current study, the K_2O/Al_2O_3 ratios observed in the Khatatba Formation sediments range from 0.11 to 0.18, with an average of 0.14 in both wells. These ratios indicate a moderate level of weathering in the area where the parent rocks were situated.

Salinity

Sr is a major component of modern-day seawater (**Turekian, 1964**). The oceanic Sr concentrations are mostly controlled by the weathering of limestones (adding Sr to the oceanic Sr pool) and diagenetic processes (responsible for the removal of Sr). Feldspars are considered to be the principal carrier of Sr in siliciclastic sedimentary rocks. The generally low concentrations of Sr in black shales are considered to be related to the low concentrations of Strontium (Sr) is a significant constituent of contemporary seawater (**Turekian, 1964**). The primary factors influencing the Sr concentrations in the ocean are the dissolution of limestones, which contributes to the Sr content, and diagenetic processes, which lead to the removal of Sr. Feldspars are regarded as the primary reservoir of Sr in siliciclastic sedimentary rocks. The relatively low levels of strontium (Sr) found in black shales are believed to be connected to the low levels of calcium (Ca) present in this particular kind of sediment **(Figs. 11, A, B; F, G)**. The Rb/Sr ratios in the published literature have been applied to infer the degree of chemical weathering that impacted the source region of the sediments (**Romer and Hahne, 2010; Taylor et al., 1983; Xu et al., 2010)**. Greater Rb/Sr ratios are indicative of significant weathering, while lower ratios suggest rather moderate weathering conditions (**Figs. 11, C, H**). In addition, Sr/Ca ratios have been used as an indicator of salinity (**Figs.11 D, I**), where low values suggest freshwater conditions and high values indicate the presence of marine salty conditions **(Chang et al., 2004; Dodd and Crisp,**

1982; Limburg, 1995; Turekian, 1955). Within the Matruh-5 and Matruh-6 wells, there is a strong correlation between high levels of strontium (Sr) and low levels of calcium (Ca) in this particular sediment type. Conversely, Rb is regarded as a detrital element that is typically concentrated in shales and siltstones. The K/Rb ratios have been shown to be useful in distinguishing different levels of salinity (**Burgan et al., 2008).**

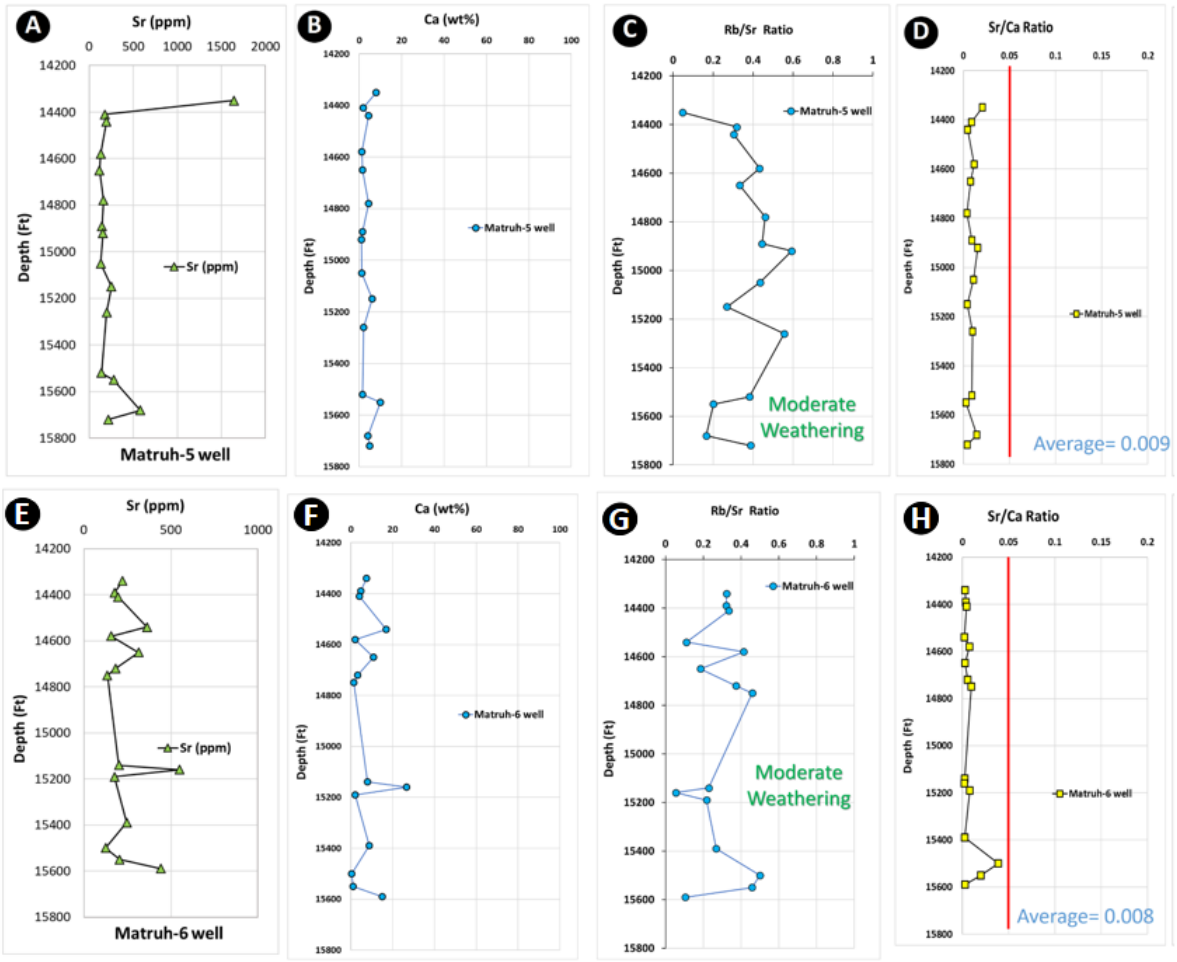

Fig. 11. Trace and Major elements concentration and ratios show the salinity and paleoenvironment conditions in Middle Jurassic Khatatba Fm at the location of Matruh-5 and Matruh-6 wells. (A-D) and (E-I) represent Sr%, Ca%, Rb/Sr ratios, and Sr/Ca ratio in Marruh-5 and Matruh-6, respectively.

5. Summary and conclusions

The deposition of the Khatatba shale is marked by a period of regional sea regression. This elucidates the increase in silicate concentration, the scarcity of carbonate, and the elevated levels of detrital metals such as iron, aluminium, titanium, and potassium. The variability in total organic carbon (TOC) and elemental data is minimal, suggesting a consistent depositional environment. The samples have moderate total organic carbon (TOC) contents, which conform to the oxic/suboxic shelf pattern. To summarize, the Upper Safa and Lower Safa members are the most significant source rock in the research area. These rock formations were formed during the Middle Jurassic period. This period was likely characterized by a very shallow marine sediments, where changes in sea level had a significant impact on the lithology of the deposited layers compared to a deeper environment. The Upper Safa and Lower Safa members were formed during a time of sea regression, resulting in the deposition of shallow marine sediments. The analyzed section of Matruh-5 and Matruh-6 wells is

distinguished by a comparatively low presence of carbonates, a significant amount of silicates, and moderate TOC values. The elemental data indicates the existence of illite, as determined by the K/Al ratio. This suggests that the climate during deposition was warm and semi-arid to arid. Vanadium to chromium ratios that are below two are seen as suggestive of environments abundant in oxygen. Similarly, Cu/Zn ratios function as indicators of redox processes, with low levels indicating oxidizing conditions. Furthermore, the samples exhibit a significant abundance of iron (Fe), titanium (Ti), and aluminium (Al), which suggests the presence of terrestrial material and an oxygen-rich deposition environment. Ultimately, it is clear that these elements were placed in shallow bottom water conditions that were poor in oxygen. The index of compositional variation (ICV) and K2O/Al2O3 ratios indicate values below 0.4, indicating low concentrations of feldspar in the initial shale and suggesting the presence of extremely mature sediments. Results indicate that V/Cr levels are below two (< 2), which suggests the presence of oxygen-rich settings. Cu/Zn ratios serve as markers of redox reactions to indicate the depositional environment settings. Additionally, K/Al and Si/Al ratios crossplot, suggesting the dominance of illite in the silicate mineral compositions present in the low carbonate deposits, which suggests a semi-arid to arid warm climate. The cross-plot of CaCo3% versus K/Al ratio suggests a shallow marine environment. The P/Al ratio, which is used as an indicator of the paleoenvironment for the tested samples in Matruh-5 and Matruh-6 wells, does not exceed 0.01. This indicates that the conditions in these wells are within the range of oxic-suboxic conditions. Moreover, crossplots of TOC% versus Fe% suggest a shallow marine depositional environment with an abundance of iron, characterized by oxic to suboxic conditions. Higher levels of Al_2O_3 suggest significant weathering and greater sediment maturity and can be attributed to the deposition of clay minerals from the water column. However, Ti concentrations can be influenced by authigenic or biogenic sources, so it is considered a more reliable indicator of the terrestrial influx compared to aluminium (Al). The relatively low levels of strontium (Sr) found in shale samples are believed to be connected to the low levels of calcium (Ca) present in this particular kind of sediment. Geologists have used Rb/Sr ratios to figure out how much chemical weathering happened in the sediments' source area. High Rb/Sr ratios mean that there was a lot of weathering. Sr/Ca ratios have been used as an indicator of salinity, where low values suggest freshwater conditions and high values indicate the presence of marine salty conditions. Within the Matruh-5 and Matruh-6 wells that were examined, there is a strong correlation between high levels of strontium (Sr) and low levels of calcium (Ca) in this particular sediment type.

Consent for publication: Author declares her consent for publication.

Conflicts of Interest:

The author affirms that she does not have any known conflicting financial interests or personal ties that could have potentially influenced the research presented in this paper.

Contribution of Authors:

The author confirms her contribution to the current article and her role as the main corresponding author. She engaged in the development, design, laboratory setup, and examination of samples, followed by data analysis, creation of drawings, organization of data, and ultimately the composition and editing of the paper.

Acknowledgements:

The author expresses deep gratitude to the Egyptian General Petroleum Corporation (EGPC) and Khalda Petroleum Company for permission and providing rock samples and well logging data for the wells analyzed in this study.

6. References

Abd El Halim, M., & Moussad, E. G. P. C. (1992) Western Desert oil and gas field's (A comprehensive overview). EGPC, ARE, Cairo, Egypt, 45-115.

Ahmed, M., (2008) Geodynamic evolution and petroleum system of Abu Gharadig Basin, north Western Desert, Egypt (No. RWTH-CONV-113041). Lehrstuhl für Geologie, Geochemieund Lagerstätten des Erdöls und der Kohle, 255 pp.

Aram, R. B., Roehl, N. L., & Feazel, C. T. (1988) Seismic stratigraphy and subsurface geology of the north–central portion of the South Umbarka Concession, Western Desert, Egypt. Phillips Petroleum Company report, 11.

Aquit, M., Kuhnt, W., Holbourn, A., Chellai, E.H., Lees, J. A., Kluth, O., Jabour, H., (2016) Complete archive of late Turonian to early Campanian

sedimentary deposition in newly drilled cores from the Tarfaya Basin, SW Morocco. Geological Society of America Bulletin 129, 137-151.

Alvarez, N. C., & Roser, B. P. (2007) Geochemistry of black shales from the Lower Cretaceous Paja Formation, Eastern Cordillera, Colombia: Source weathering, provenance, and tectonic setting. Journal of South American Earth Sciences 23, 271-289.

Avseth, P., & Bachrac, R. (2005) Seismic properties of unconsolidated sands: Tangential stiffness, Vp/Vs ratios and diagenesis. In SEG International Exposition and Annual Meeting SEG-2005.

Barbera, G., Mazzoleni, P., Critelli, S., Pappalardo, A., Lo Giudice, A., & Cirrincione, R. (2006) Provenance of shales and sedimentary history of the Monte Soro Unit, Sicily. Periodico di Mineralogia, 75(2-3), 313-330.

Brumsack, H. J. (1991) Inorganic geochemistry of the German 'Posidonia Shale': palaeoenvironmental consequences. Geological Society, London, Special Publications, 58(1), 353-362.

Burgan, A. M., Ali, C. A., & Tahir, S. H. (2008) Chemical composition of the Tertiary black shales of West Sabah, East Malaysia. Chinese Journal of Geochemistry, 27, 28-35.

Calvert, S. E., & Pedersen, T. F. (2007) Chapter fourteen elemental proxies for palaeoclimatic and palaeoceanographic variability in marine sediments: interpretation and application. Developments in Marine Geology, 1, 567-644.

Campbell, F. A., & Williams, G. D. (1965) Chemical composition of shales of Mannville group (Lower Cretaceous) of central Alberta, Canada. AAPG Bulletin, 49(1), 81-87.

Cox, R., Lowe, D. R., & Cullers, R. L. (1995) The influence of sediment recycling and basement composition on evolution of mudrock chemistry in the southwestern United States. Geochimica et Cosmochimica Acta, 59(14), 2919-2940.

Cullers, R. L., & Podkovyrov, V. N. (2000) Geochemistry of the Mesoproterozoic Lakhanda shales in southeastern Yakutia, Russia: implications for mineralogical and provenance control, and recycling. Precambrian Research, 104 (1-2), 77-93.

Daher, S. B., Nader, F. H., Müller, C., & Littke, R. (2015) Geochemical and petrographic characterization of Campanian–Lower Maastrichtian calcareous petroleum source rocks of Hasbayya, South Lebanon. Marine and Petroleum Geology, 64, 304-323.

Dean, W. E., & Arthur, M. A. (1989) Iron-sulfur-carbon relationships in organic-carbon-rich sequences; I, Cretaceous Western Interior Seaway. American Journal of Science, 289(6), 708-743.

Dodd, J. R., & Crisp, E. L. (1982) Non-linear variation with salinity of Sr/Ca and Mg/Ca ratios in water and aragonitic bivalve shells and implications for paleosalinity studies. Palaeogeography, Palaeoclimatology, Palaeoecology, 38 (1-2), 45-56.

Dolson, J. C., Boucher, P. J., and Shann, M. V., (2000) Exploration Potential in the Offshore Mediterranean, Egypt-Perspectives from the Context of Egypt's Future Resources and Business Challenges. In EAGE Conference on Geology and Petroleum Geology of the Mediterranean and Circum-Mediterranean Basins. EAGE-109.

Dolson, J. C., Shann, M. V., Matbouly, S. I., Hammouda, H., Rashed, R.M., (2001) Egypt in the twenty-first century: petroleum potential in offshore trends. GeoArabia 6, 211–230.

EGPC (1992) Western Desert, Oil and Gas Fields, A comprehensive Overview. EGPC, 11th Petroleum Exploration Production Conference, Cairo, Egypt, 431.

El Atfy, H., & Ghassal, B. I., (2022) Advances in Petroleum Source Rock Characterizations: Integrated Methods and Case Studies: a Multidisciplinary Source Rock Approach. Springer.

Espitalie, J., Deroo, G., Marquis, F., (1985). Rock-Eval pyrolysis and its applications. Revue De L

Institut Francais Du Petrole 40, 563-579.

Ferriday, T., & Montenari, M. (2016) Chemostratigraphy and chemofacies of source rock analogues: A high-resolution analysis of black shale successions from the Lower Silurian Formigoso Formation (Cantabrian Mountains, NW Spain). In Stratigraphy & timescales, 1, 123-255.

Ghassal, B.I., Littke, R., Sachse, V., Sindern, S., Schwarzbauer, J., (2016) Depositional Environment and Source Rock Potential of Upper Albian to Turonian sedimentary rocks of the Tarfaya Basin, Southwest Morocco. Geologica Acta, 14, 419-441.

Ghassal, B. I., Littke, R., El Atfy, H., Sindern, S., Scholtysik, G., El Beialy, S., & El Khoriby, E. (2018) Source rock potential and depositional environment of Upper Cretaceous sedimentary rocks, Abu Gharadig Basin, Western Desert, Egypt: An integrated palynological, organic and inorganic geochemical study. International Journal of Coal Geology, 186, 14-40.

Gordon, E. S., and Goñi, M. A., (2003) Sources and distribution of terrigenous organic matter delivered by the Atchafalaya River to sediments in the northern Gulf of Mexico. Geochimica et Cosmochimica Acta, 67(13), 2359-2375.

Guiraud, R., Bosworth, W., (1997) Senonian basin inversion and rejuvenation of rifting in Africa and Arabia: synthesis and implications to plate-scale tectonics. Tectonophysics, 282, 39-82.

Guiraud, R., Issawi, B., Bosworth, W., Ziegler, P.A., Cavazza, W., Robertson, A.H.F., Crasquin-Soleau, S., (2001) Phanerozoic history of Egypt and surrounding areas. Peri-Tethys Memoir, 6, 469–509.

Hantar, G., (1990) North Western Desert. In: R. Said (Ed.), The Geology of Egypt. A.A. Balkema, Rotterdam, Brookfield, 293-319.

Harnois L., (1988) The CIW index: a new chemical index of weathering. Sedimentary Geology, 55, 319-322.

Herron, M. M., (1988) Geochemical classification of terrigenous sands and shales from core or log data. Journal of Sedimentary Research, 58 (5), 820-829.

Hussein, I. M., and Abd-Allah, A. M. A. (2001) Tectonic evolution of the northeastern part of the African continental margin, Egypt. Journal of African Earth Sciences, 33 (1), 49-68.

Khalda Petroleum Company, 2010: Internal unpublished report.

Kolonic, S., Sinninghe Damsté, J. S., Böttcher, M. E., Kuypers, M. M. M., Kuhnt, W., Beckmann, B. , and Wagner, T. (2002) Geochemical Characterization of Cenomanian/Turonian Black Shales From the Tarfaya Basin (SW Morocco) Relationships between Palaeoenvironmental Conditions and Early Sulphurization of Sedimentary Organic Matter 1. Journal of Petroleum Geology, 25 (3), 325-350.

Limburg, K. E. (1995) Otolith strontium traces environmental history of subyearling American shad Alosa sapidissima. Marine Ecology Progress Series, 25-35.

Machhour L., Philip J., Oudin J.L., (1994) Formation of Laminite deposits in anaerobic-dysaerobic marine environments. Marine. Geology. 117, 287-302.

Mansour, A., Gentzis, T., Tahoun, S. S., Ahmed, M. S., Gier, S., Carvajal-Ortiz, H., and Wang, J. (2023) Near equatorial paleoclimatic evolution and control on organic matter accumulation during the Cenomanian in the Abu Gharadig Basin, southern Tethys: Insights from palynology, organic petrography, and geochemistry. International Journal of Coal Geology, 270, 104221.

Meshref, W. M., and H. Hammouda. (1990) "Basement tectonic map of Northern Egypt." Proceedings of the EGPC 9th Exploration and Production Conference, Cairo. Egyptian General Petroleum Corporation Bulletin. 1.

Meshref, W. M. (1999) Cretaceous tectonics and its impact on oil exploration in northern Egypt. Geological Society of Egypt Special Publication., (2) 199-244.

Moustafa, A.R. (2008) Mesozoic–Cenozoic basin evolution in the northern Western Desert of Egypt, In: Salem, M., El-Arnauti, A., and Saleh, A. (eds.): 3rd Symposium on the Sedimentary Basins of Libya, the Geology of East Libya, 3, 29–46.

Moustafa, A.R. (2020) Mesozoic-Cenozoic deformation history of Egypt. The Geology of Egypt, 253-294.

Murray, R. W., and Leinen, M. (1996) Scavenged excess aluminum and its relationship to bulk titanium in biogenic sediment from the central equatorial Pacific Ocean. Geochimica et Cosmochimica Acta, 60 (20), 3869-3878.

Nagarajan, R., Madhavaraju, J., Nagendra, R., and Armstrong-Altrin, J. S., & Moutte, J. (2007) Geochemistry of Neoproterozoic shales of the Rabanpalli Formation, Bhima Basin, Northern Karnataka, southern India: implications for provenance and paleoredox conditions. Revista Mexicana de Ciencias Geológicas, 24 (2), 150-160.

Nesbitt H. W., and Young G. M., (1982) Early Proterozoic climate and plate motions inferred from major element chemistry of lutites. Nature, 299, 715-717.

Niebuhr, B. (2005) Geochemistry and time-series analyses of orbitally forced Upper Cretaceous marl–limestone rhythmites (Lehrte West Syncline, northern Germany). Geological Magazine, 142, 31-55.

Okunlola, O. A., Adeigbe, O. C., & Oluwatoke, O. O. (2009) Compositional and petrogenetic features of schistose rocks of Ibadan area, southwestern Nigeria. Earth Sciences Research Journal, 13 (2), 119-133.

Peters, K. E. (1986) Guidelines for evaluating petroleum source rock using programmed pyrolysis. AAPG Bulletin., 70, 318-329.

Peters, K. E., and Cassa, M. R. (1994) Applied source rock geochemistry: Chapter 5: Part II. Essential elements.

Peters, K. E., Walters, C. C., Moldowan, J. M. (2005) The Biomarker Guide. Cambridge University Press, 2, 1155.

Romer, R. L., and Hahne, K. (2010) Life of the Rheic Ocean: scrolling through the shale record. Gondwana Research, 17 (2-3), 236-253.

Sachse, V. F., Littke, R., Jabour, H., Schümann, T., Kluth, O. (2012) Late Cretaceous (late Turonian, Coniacian and Santonian) petroleum source rocks as part of an OAE, Tarfaya Basin, Morocco. Marine and Petroleum Geology, 29, 35-49.

Schroder, S., and Grotzinger, J. P. (2007) Evidence for anoxia at the Ediacaran–Cambrian boundary: the record of redox-sensitive trace elements and rare earth elements in Oman. Journal of the Geological Society, 164 (1), 175-187.

Schultz, R. B. (2004) Geochemical relationships of Late Paleozoic carbon-rich shales of the Midcontinent, USA: a compendium of results advocating changeable geochemical conditions. Chemical Geology, 206 (3-4), 347-372.

Shahin, A. N., Shehab, M. M., Mansour, H. F. (1986) Quantitative evaluation and timing of petroleum generation in Abu Garadig basin, Western Desert, Egypt. Proceedings of 8th Petroleum Exploration and Production Conference. The Egyptian General Petroleum Corporation, EGPC, Cairo, 1-18.

Sestini, G. (1994) “Egypt,”. Regional petroleum Geology of the world. Editor H. Kulke (Berlin: Gebruder Borntraeger), 3, 23–46.

Sultan, N., Halim, M. A. (1988) Tectonic framework of northern Western Desert, Egypt and its effect on hydrocarbon accumulations. In proceedings of the EGPC 9th exploration and production conference, Cairo. Egyptian General Petroleum Corporation Bulletin, 2, 1–19

Taylor, S. R., McLennan, S. M., and McCulloch, M. T. (1983) Geochemistry of loess, continental crustal composition and crustal model ages. Geochimica et Cosmochimica Acta, 47 (11), 1897-1905.

Taylor, G. H., Teichmüller, M., Davis, A., Diessel, C. F. K., Littke, R., Robert, P. (1998) Organic

Petrology. Stuttgart, Borntraeger, 704.

Tribovillard, N., Algeo, T. J., Lyons, T., Riboulleau, A., 2006. Trace metals as paleoredox and paleoproductivity proxies: an update. Chemical Geology 232, 12–32.

Turekian, K. K. (1957) Additional trace element analyses of standard granite G-1 and standard diabase W-1. Science, 126 (3277), 745-746.

Turekian, K. K. (1964) The marine geochemistry of strontium. Geochimica et Cosmochimica Acta., 28 (9), 1479-1496.

Turekian, K. K., and Kulp, J. L. (1956) The geochemistry of strontium. Geochimica et Cosmochimica Acta, 10 (5-6), 245-296.

Wei, G., Liu, Y., Li, X., Shao, L., and Liang, X. (2003) Climatic impact on Al, K, Sc and Ti in marine sediments: evidence from ODP Site 1144, South China Sea. Geochemical Journal, 37 (5), 593-602.

Wignall, P. B. (1994) Mudstone Lithofacies in the Kimmeridge Clay Formation, Wessex Basin, Southern England: Implications for the Origin and Controls of the Distribution of Mudstones: Journal of Sedimentary Research, 64 (4).

Wohlfarth, B., Blaauw, M., Davies, S. M., Andersson, M., Wastegård, S., Hormes, A., and Possnert, G. (2006) Constraining the age of Lateglacial and early Holocene pollen zones and tephra horizons in southern Sweden with Bayesian probability methods. Journal of Quaternary Science: Published for the Quaternary Research Association, 21(4), 321-334.

Xu, H., Liu, B., & Wu, F. (2010) Spatial and temporal variations of Rb/Sr ratios of the bulk surface sediments in Lake Qinghai. Geochemical Transactions, 11(1), 1-8.

Zhang, Y., He, Y., Zhou, W., Mo, G., Chen, H., and Xu, T. (2023) Review on the elemental analysis of polymetallic deposits by total-reflection X-ray fluorescence spectrometry. Applied Spectroscopy Reviews, 58 (6), 428-441.

البيئة الترسيبية والمناخ القديم للصخور الرسوبية الجوراسية الوسطى في حوض مطروح، الصحراء الشمالية الغربية، مصر

ولاء عواد علي

قسم جيولوجيا البترول، كلية علوم البترول والتعدين، جامعة مطروح، ٥١٥١١، مطروح، مصر

تبحث هذه الدراسة في البيئة الترسيبية والظروف المناخية القديمة لتكوين الخطاطبة الجوراسي الأوسط في حوض مطروح، شمال غرب مصر، والذي يمثل منتجًا إقليميًا مهمًا للغاز في منطقة شرق البحر الأبيض المتوسط. يتميز تكوين الخطاطبة بخصائص المصدر والخزان المزدوج في الموقع، حيث تشكل تقلبات الفتاتات الناعمة والخشنة مصادر داخل التكوين (الليثولوجيا "السحنة الصخرية"، الصخر الزيتي وأحجار الغرين الطينية)، حيث نسبة الكربون العضوي الكلي بالوزن: ٠,٨٨% - ١٢,٩٨%، بمتوسط ٢,٩٥%، و ٠,٨٠%-٦,٩٩%، بمتوسط ٢,٢٦% في بئر (مطروح-٥) وبئر (مطروح-٦) على التوالي. ومع ذلك، فقد ترسبت صخور مكمن (الليثولوجي: الحجر الرملي) في ظروف شبه جافة وشبه رطبة. ويرتبط هذا الأداء المزدوج لتكوين الخطاطبة في الموقع بالتغير في مستوى سطح البحر في حوض المتوسط القديم والتغيرات المناخية خلال العصر الجوراسي الأوسط. حيث تسببت الصدوع في حوض المتوسط خلال أواخر العصر الجوراسي وأوائل العصر الطباشيري في احداث هبوط، والذى ترتب عليه نُضج صخور المصدر.

لدراسة ظروف المنشأ والترسيب المسئولة عن تراكم الرواسب العضوية الغنية والفقيرة في تكوين الخطاطبة بحوض مطروح. تم استخدام البيانات الجيوكيميائية غير العضوية والجيوفيزيائية لتفسير البيئة الترسيبية. بدراسة العينات الفتاتية لتكوين الخطاطبة تبين ان مستوى التجوية متوسط في الآبار المستهدفة للدراسة الحالية حيث، (المؤشر الكيميائي للتغيير CIA =: متوسط ٧٠ ومتوسط ٥٩، مؤشر التباين الكيميائي = ICV: متوسط ١,١ ومتوسط ١,٨، كيميائي مؤشر التجوية = CIW: متوسط ٧٧,٨ ومتوسط ٦٤,٧) لبئر مطروح-٥ ومطروح-٦ على التوالي. علاوة على ذلك، تم استخدام نسب Rb/Sr (متوسط ٠,٣٦، ٠,٢٩ في بئر مطروح ٥ ومطروح ٦، على التوالي) لمعرفة مقدار التجوية الكيميائية التي حدثت في المنطقة مصدر الرواسب، والتي تُصنف على أنها تجوية معتدلة متوسطة.

متوسط نسب اكاسيد العناصر K2O/Al2O3 يبلغ تقريبا ٠,١٤ في كلا البئرين، أي أقل من ٠,٤، مما يشير إلى نضج هذه الرواسب. بالإضافة إلى أنه تم استخدام نسب K2O/Al2O3 أيضًا لاستنتاج التجوية الكيميائية في الآبار المستهدفة، حيث تشير القيم إلى مستوى معتدل من التجوية في المنطقة التي تقع فيها الصخور الأم أيضًا. داخل بئري مطروح-٥ ومطروح-٦، هناك علاقة قوية بين المستويات العالية من السترونشيوم (Sr) والمستويات المنخفضة من الكالسيوم (Ca) في هذا النوع من الرواسب بالتحديد من تكوين الخطاطبة. وهذا يفسر سبب تراكم هذه الرواسب في بيئات الدلتا التي يسيطر عليها المد والجزر وعلى أساس اختلاف نسب الملوحة، حيث تم استخدام نسب Sr/Ca كمؤشر للملوحة. ولهذا، فإن الارتباطات السلبية لـعنصر Ti مع Al في بئر مطروح-٥ (وحدة الصفا علوى: R^2= 0.1139 ؛ وحدة الصفا السفلى: R^2=0.0007) تُشير إلى عدم وجود ارتباط مع معادن طين الألومينوسيليكات. في حين أن الارتباطات الإيجابية القوية لـ Ti مع Al في بئر مطروح-٦ (وحدة الصفا العلوى: R^2= 0.858؛ وحدة الصفا السفلى: R^2= 0.946) تشير إلى ارتباط معادن الألومينوسيليكات. حدث ترسب تكوين الخطاطبة خلال ظروف شبه جافة نسبيًا (Sr/Cu: بمتوسط ١٠,٠٣ ؛ ١١,٣٣ Rb/Sr: بمتوسط ٠,٣٦ ؛ ٠,٢٩)، والتي تميزت بمدخلات شديدة الارتفاع شملت (معدل تدفق الرواسب (Al/Ca): بمتوسط. (٤,٤٧ بئر مطروح-٥، ٣,٨٧ بئر مطروح-٦). أدت ظروف الملوحة الطبيعية المتراكمة في الغالب تحت ظروف الأكسدة إلى نقص الأكسجين، حيث بلغت النسبة (MgO/Al_2O_3*١٠٠): متوسط ٨,٤٨، فى بئر مطروح-٥؛ و١١,٣٧، في بئر مطروح-٦)، والنسبة ((V/(V + Ni): متوسط ٠,٥٨ في بئر مطروح-٥، ومتوسط ٠,٣٢ في بئر مطروح-٦)، وبلغت نسبة Zn/Cu: متوسط. ٠,٣٤ في بئر مطروح-٥؛ ومتوسط ٠,٢٧ بئر مطروح - ٦).

الكلمات المفتاحية: البيئة الترسيبية، المناخ القديم، تحليل عناصر XRF، الصخور المصدرية، حوض الخطاطبة بمطروح.